



# CHALMERS

---



## Vehicle Motion Priority

### Motion Analysis of Deceleration While Cornering

Master's thesis in Automotive Engineering

ROBERT SAMEFORS

KARL-JOHAN HAGELIN



MASTER'S THESIS IN AUTOMOTIVE ENGINEERING

# Vehicle Motion Priority

Motion Analysis of Deceleration While Cornering

ROBERT SAMEFORS  
KARL-JOHAN HAGELIN

Department of Applied Mechanics

*Division of Vehicle Engineering and Autonomous Systems*  
*Vehicle Dynamics Group*

CHALMERS UNIVERSITY OF TECHNOLOGY

Göteborg, Sweden 2016

Vehicle Motion Priority  
Motion Analysis of Deceleration While Cornering  
ROBERT SAMEFORS  
KARL-JOHAN HAGELIN

© ROBERT SAMEFORS, KARL-JOHAN HAGELIN, 2016

Master's thesis 2016:50  
ISSN 1652-8557  
Department of Applied Mechanics  
*Division of Vehicle Engineering and Autonomous Systems*  
*Vehicle Dynamics Group*  
Chalmers University of Technology  
SE-412 96 Göteborg  
Sweden  
Telephone: +46 (0)31-772 1000

Cover:  
Saab 9-3 EV Prototype in motion, courtesy of John Andersson

Chalmers Reproservice  
Göteborg, Sweden 2016

Vehicle Motion Priority  
Motion Analysis of Deceleration While Cornering  
Master's thesis in Automotive Engineering  
ROBERT SAMEFORS  
KARL-JOHAN HAGELIN  
Department of Applied Mechanics  
*Division of Vehicle Engineering and Autonomous Systems*  
*Vehicle Dynamics Group*  
Chalmers University of Technology

## ABSTRACT

This thesis has investigated the wanted motion in a scenario where contradictory motions occur, as a step towards integrated control of vehicle motion. The chosen scenario was the case of deceleration while cornering. Two contradictory motions were identified; longitudinal deceleration and path following. If different motions are desired, this could lead to clear contradictory intentions on a vehicle level, due to interventions from different systems and actuators. The introduction of Advanced Driver Assisting System (ADAS) and autonomous functionality in an already complicated function architecture may lead to contradictory intentions if the systems do not have a common view of the vehicle state, especially since the systems do not share a common reference model. Traditionally, the conventional brake system has the top priority to decrease speed, but with the introduction of autonomous systems in the function architecture this might lead to severe consequences if no clear prioritization is set between different system and function intentions. However, a fixed prioritization cannot be set due to the large variation of possible scenario, which is the driving force behind an integrated vehicle motion control. A control, which has a common view of the vehicle state and is deciding a wanted motion is therefore desired. This controller aims at removing the boundaries between different systems and is therefore reducing the function architecture complexity.

The chosen scenario was investigated with the brakes and the steering as the primary actuators, where the total braking distance and off-tracking were the observed measurements. The initial velocity and the allowed off-tracking varied during the investigation to observe what could be gained in terms of braking distance, velocity and stopping time by allowing a certain off-tracking compared to a more strict path following constraint. An investigation with a two track model was performed via optimal control with the optimal control package PROPT in MATLAB/SIMULINK. The investigation was made with both the initial conditions for a constant velocity steady state cornering and the initial conditions representing quasi-steady state braking. This was done to capture both the transient behavior from a step braking/steering and the case of quasi-steady braking, where the braking has already been initiated, for determining the major players in maximizing longitudinal deceleration and following the intended path. The sensitivity of the optimal solution was tested with respect to road adhesion level and side slip constraint, to observe the robustness of the optimal solution.

The problem at hand was also solved with a particle representation to find similarities that can be useful in a possible future vehicle application due to its real time computation requirements. The comparison between the quasi-steady state braking and the particle representation showed similarities in lane utilization and in the direction of the total force vector. Therefore, a simple controller was derived from the friction circle, based on the wanted lateral acceleration calculated with the optimal path from a particle representation.

The results show that the braking distance can be decreased for the optimal control solution with an allowed off-tracking. The velocity can be reduced with respect to travelled distance and a minor reduction in stopping time was found. The decrease in braking distance, velocity and stopping time might yield a safety benefit to future vehicles. The optimal solution showed that a need of lateral velocity for providing sufficient lateral force was necessary to maximize the longitudinal deceleration. This was observed both from the transient behavior and the quasi-steady braking case. The simple brake controller showed varying results compared to the optimal control of the two track model which indicates that future work should be performed, regarding the wanted curvature during the intervention.

Keywords: Vehicle Dynamics, Vehicle motion, Motion priority, Integrated control, Integrated vehicle motion control, Braking, Steering, Braking distance, Off-tracking, Lane utilization, Optimal control, Pseudo spectral collocation method, PROPT, Safety



## PREFACE

This thesis has been performed in accordance with the requirements to acquire the Master of Science degree of Automotive Engineering at Chalmers University of Technology, Gothenburg, in cooperation with National Electric Vehicle Sweden AB (NEVS), Trollhättan. The project was conducted from January to June 2016.

## ACKNOWLEDGEMENTS

We would like to thank Johan Hägnander at National Electrical Vehicle Sweden for his support and guidance, during discussions and weekly meetings, regarding integrated vehicle motion control and the intentions of such an implementation in a future vehicles. We also want to thank Adithya Arikere and Mathias Lidberg for guidance and support during the project regarding vehicle dynamics, optimization and report writing, which has been of major importance for the outcome of the thesis.

We would also like to thank the great people at the company NEVS for their warm welcome and for making us feel at home during the project. Thanks to the restaurant Saltes for providing us with good food when our lunchboxes were left at home. A special thanks to Victor Hermansson and Kedarnath Moparthi for enduring our company during the commute between Gothenburg and Trollhättan.

Finally, we would like to thank our families and friends for their support and encouragement during the project of *Vehicle Motion Priority*.



# NOMENCLATURE

## Symbols

$L$	Wheelbase [m]
$h$	Center of gravity height [m]
$h'$	Distance from center of gravity to roll axis [m]
$w$	Track width [m]
$s$	Half of track width [m]
$a_1$	Distance from front axle to center of gravity [m]
$a_2$	Distance from rear axle to center of gravity [m]
$a_x$	Longitudinal acceleration [m/s <sup>2</sup> ]
$a_y$	Lateral acceleration [m/s <sup>2</sup> ]
$\delta$	Steer angle on front
$\delta_{fr}$	Steer angle on front right
$\delta_{fl}$	Steer angle on front left
$m$	Vehicle mass
$v_x$	Longitudinal velocity
$v_y$	Lateral velocity
$V$	Total velocity
$\dot{v}_x$	First order time derivative of longitudinal velocity
$\dot{v}_y$	First order time derivative of lateral velocity
$\psi$	Heading angle (yaw angle)
$r$	Yaw rate
$\dot{r}$	Yaw acceleration
$\beta$	Side slip angle
$\varphi$	Roll angle
$\dot{\varphi}$	Roll rate
$\ddot{\varphi}$	Second order time derivative of the roll angle
$\theta$	Pitch angle
$\dot{\theta}$	Pitch rate
$\ddot{\theta}$	Second order time derivative of the pitch angle
$\alpha_{ij}$	Lateral slip angle
$d_b$	Braking distance
$d_{off}$	Allowed off-tracking
$v_{lim}$	Maximum corner entry velocity
$v_{thr}$	Velocity threshold for optimization
$\beta_{lim}$	Maximum side slip angle for optimization

## Subscripts

$F_{x1l}$	Longitudinal force on front, left wheel
$F_{x1r}$	Longitudinal force on front, right wheel
$F_{x2l}$	Longitudinal force on rear, left wheel
$F_{x2r}$	Longitudinal force on rear, right wheel
$F_{y1l}$	Lateral force on front, left wheel
$F_{y1r}$	Lateral force on front, right wheel
$F_{y2l}$	Lateral force on rear, left wheel
$F_{y2r}$	Lateral force on rear, right wheel

## Abbreviations

ADAS	Advanced Driver Assistance System
ABS	Anti-Locking Brakes
AEB	Autonomous Emergency Braking
AIS	Abbreviated Injury Scale
CoG	Center of gravity
EBD	Electronic Brake Force Distribution
ESC	Electronic Stability Control
FLW	Front Left Wheel
FRW	Front Right Wheel
RLW	Rear Left Wheel
RRW	Rear Right Wheel
IMU	Inertial measurement Unit
WAD	Whiplash Associated Disorder
TTC	Time to Collision
OCP	Optimal Control Particle
OCB	Optimal Control Braking (Vehicle Model)
OCBS	Optimal Control Braking and Steering (Vehicle Model)
FBP	Fixed Brake Proportioning (Reference Braking System)
FPBS	Fixed Brake Proportioning with Steering (Reference Braking System)
AMR	Acceleration Magnitude Reference (Controller)

# CONTENTS

<b>Abstract</b>	<b>i</b>
<b>Preface</b>	<b>iii</b>
<b>Acknowledgements</b>	<b>iii</b>
<b>Nomenclature</b>	<b>v</b>
<b>Contents</b>	<b>vii</b>
<b>1 Introduction</b>	<b>1</b>
1.1 Background . . . . .	1
1.2 Problem Definition . . . . .	3
1.3 Objective . . . . .	4
1.4 Delimitation . . . . .	4
<b>2 Vehicle Modeling</b>	<b>5</b>
2.1 Coordinate System . . . . .	5
2.2 Two Track Model . . . . .	6
2.2.1 Tire Modelling . . . . .	7
<b>3 Decelerating in a Curve</b>	<b>9</b>
3.1 Optimal Control Preliminaries . . . . .	10
3.2 State of the Art Representation Using Fixed Brake Proportion with Optimal Steering Input . . . . .	10
3.3 Individual Wheel Braking with Optimal Control . . . . .	12
3.3.1 Formulation of the Optimal Control Problem . . . . .	12
3.4 Analysis of Braking Strategies shows Transient Behaviour . . . . .	13
3.5 Neglecting the Transient Phase Yields Quasi-Steady State Solution . . . . .	20
3.6 Optimal Control Results Show Trade-off in Braking Distance versus Off-tracking . . . . .	25
3.6.1 Decreased Braking Distance by Introducing an Allowed Off-Tracking . . . . .	25
3.6.2 Transient Phase Shows Larger Gains in Braking Distance, Velocity Decrease and Stopping Time . . . . .	28
<b>4 Control Design</b>	<b>29</b>
4.1 Optimal Control with Particle Representation . . . . .	29
4.2 Particle Representation Yields Strategy for Control . . . . .	32
4.2.1 Open Loop Implementation of the Acceleration Magnitude Reference . . . . .	34
<b>5 Control Performance Evaluation</b>	<b>35</b>
<b>6 Discussion</b>	<b>39</b>
<b>7 Conclusions &amp; Future Work</b>	<b>42</b>
<b>References</b>	<b>44</b>
<b>Appendix</b>	<b>46</b>
<b>A Vehicle Data</b>	<b>46</b>
<b>B Vehicle System Modelling</b>	<b>47</b>
B.1 Coordinate System Transformation . . . . .	47
B.2 Vehicle Dynamics Theory . . . . .	47
<b>C Sensitivity Analysis Regarding Side Slip &amp; Friction Variations</b>	<b>54</b>



# 1 Introduction

## 1.1 Background

Active safety systems in a modern vehicle try to mitigate or avoid accidents in a near future. Recent advances in sensors, computing power, decision making, etc., have enabled implementation of active safety systems in mass produced cars. The driver is accounted for being the critical reason in a causal chain of events in over 90% of all crash situations [1]. The human factor is therefore a major cause of accidents. However, this does not imply that the driver is responsible for the collision; the environment is claimed to be responsible for 50% of the accidents [2]. Advanced Driver Assistance Systems (ADAS), that aim at relieving the driver from his or her tasks, have therefore a large potential to avoid crashes and thereby also reduce the number of fatalities in the road transportation sector to reach both international and national target values like the Swedish approach of *Vision Zero* [3]. The fatalities, number of accidents and the number of injuries in the EU has decreased the past few years [4], partially due to active safety systems. However, the risk of dying and the total number of fatalities is much greater within the road transportation sector compared to other transportation sectors [5], which means that much can be done when it comes to safety improvements.

With fully or semi-autonomous vehicles on the rise the vehicle itself needs a clear view of its surroundings and operational limits, both on vehicle and actuator level. The vehicle is therefore in need of more information than ever before. The active safety systems that exists today concerns both comfort, safety and performance. However, the increasing amount of hardware and software for controlling the vehicle motion is also increasing the complexity of the function architecture. This since each system or function aims at controlling one motion, other motions might be affected [6]. This can lead to contradictions on a vehicle level, which in total has six degrees of freedom that should be controlled. Examples of some driver assisting systems of today are Autonomous Emergency Brake (AEB) and Electronic Stability Control (ESC), which works together with Anti-lock Braking System (ABS) and Electronic Brake Force distribution (EBD).

The intention of the Automatic Emergency Brake system, AEB, is to avoid or mitigate an imminent collision. The AEB system addresses rear end collisions, where the host vehicle is the striking vehicle, which are one of the most common road accidents of today [7]. Neck injuries with low severity on the *Abbreviated Injury Scale*, AIS, are one of the most common injuries in rear end collisions. However, even low severity injuries, like AIS1 neck injuries, have proven to be one of the biggest causes of disabilities due to road accidents [8]. The AEB system has also a large safety benefit when it comes to mitigate severe injuries in road accidents. The potential safety benefit regarding AIS6 injuries is expected to be  $\sim 30\%$  for an AEB equipped vehicle compared to a vehicle without AEB [9]. A functionality where the vehicle applies maximum brake pressure, without driver intervention, can therefore be regarded as one of the most important driver assistant systems of today. The AEB operates continuously to evaluate the risk of a possible imminent collision by estimating time gap and distance to the lead object. A typical measure for deciding if an intervention shall be performed is *Time To Collision*, TTC. TTC is a range measurement including distance between host vehicle and objective vehicle together with the relative velocity [10]. The AEB shall perform an intervention as late as possible to avoid nuisances for the driver and passengers, but must still be able to prevent or reduce the severity of an imminent accident.

The Electronic Stability Control, ESC, aims at controlling the yaw motion of a vehicle by controlling the slip ratio on individual wheels. The main purpose of the ESC is to limit the side slip angle, in order to decrease the risk of vehicle skidding. The stability control can be achieved through different actuators. The most commonly mentioned in order to remain stable is differential braking i.e. brake based ESC. The ESC architecture can be described as two level control systems; upper control and lower control level [11]. The upper controller aims at determining the yaw moment to correct the deviation in yaw motion, whereas the lower control decides the brake pressure to meet the calculated yaw moment provided by the upper control. The upper control controls the deviation in yaw rate and slip angle. The nominal yaw rate (target yaw rate) can be calculated using the intention of the driver, the vehicle characteristics and the current state of the vehicle.

The Anti-lock Braking System, ABS, attempts to minimize the braking distance while preserving steer ability during a braking maneuver [10]. The ABS system is a standard safety system in vehicles and it is found to decrease the risk of crashing into a leading vehicle. The risk can be reduced with approximately  $32\%$  ( $\pm 8\%$ )

compared to a non ABS equipped vehicle on wet road conditions [12]. The ABS is engaged during harsh braking maneuvers to avoid wheel lock up. The ABS keeps the slip ratio at a certain level by regulating the brake torque on the wheels. The adjustment of the brake pressure is decided by monitoring of the wheel speed and comparing it to the vehicle speed. The ABS can use a sub-function called *Select low*, to maintain stability during the braking. *Select low* represents a brake pressure adjustment based on the wheel that is closest to locking the wheel i.e. select the lowest pressure [10]. *Select low* could be beneficial when braking on split  $\mu$ , but could however decrease the effectiveness of the ABS with respect to minimizing the braking distance. Using the select low function it appears that there is no distinct difference between Anti-lock Brake System and an Electronic Brake Distribution system, EBD and it is often regarded as a combined feature [10]. Another way of remain stable can be done by delaying the pressure in the brake calipers to receive a yaw-moment build-up delay [13]. The yaw moment delay could be beneficial in order for the driver to have enough time to begin a counter steer maneuver [14].

A problem arises when all these different brake based systems demands contradictory interventions. Since the vehicle control systems and actuators are controlled independently, in the sense that they use different reference models and sensors for determining if an intervention is to be made. These systems have limited communication with other systems regarding their intentions and view of different situations. This type of function architecture creates situations and scenarios where different systems or subsystems can have conflicting intentions or interests which can have a non-optimal or even fatal outcome if these systems are not strictly hierarchically structured. A priority can however not be set without knowledge of the surroundings due to the large variation of scenarios that can occur on the roads. The vehicles of the future will therefore benefit from having a more sophisticated integrated vehicle motion control. This control, based on a vehicle motion priority, will create a possibility of coordinating multiple actuators to reach a desired motion. This will also separate the decision making and the actuating and create a more clear function architecture. What is meant by integrated control is that the arbitration, or even alternation, between different motions should happen at a higher level in the function architecture. Moving the decision making higher up the hierarchy could remove contradictory intentions at lower levels. With this follows the idea of having a master reference model combining all sensors to give a single, clear view of surroundings and the state of the vehicle. A scenario where the different motion intentions are contradictory is the braking in corner scenario. The host vehicle is traveling in a corner when an object appears in the host vehicles path which triggers a brake intervention to avoid a possible collision. However, a harsh brake intervention induces a path deviation if too much of the road adhesion is allocated to longitudinal deceleration.

## 1.2 Problem Definition

The foundation of the problem at hand is based on the fact that the increasing number of functions in vehicles increases complexity and put high demands on the function architecture. An example of a function architecture of today is seen in Figure (1.1). Traditionally, the braking, steering and propulsion have been separated branches in the function architecture, with interfaces between them, where the braking has been prioritized. The introduction of autonomous systems has increased the demands on more interfaces and an increase in possible interventions by different systems. The intentions from a large variety of systems and ECU's will create situations where contradictory wanted motions are requested.

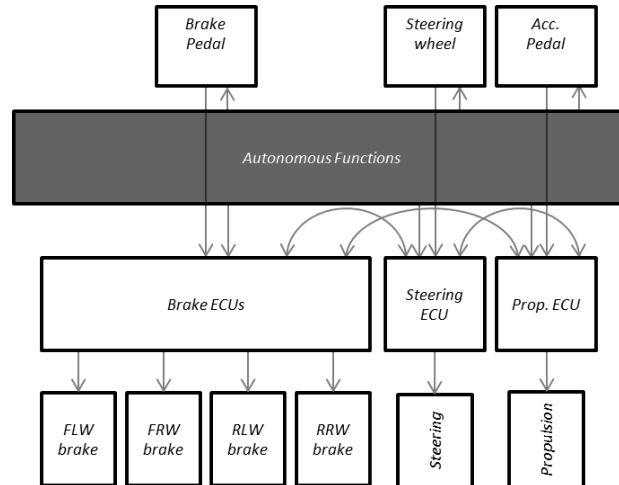


Figure 1.1: *Example function architecture.*

This is the reason for migrating towards integrated vehicle motion control, where the wanted motion is centrally determined. This thesis has evaluated the positive effects of an integrated motion control in the scenario of decelerating while cornering. The result with the architecture depicted in Figure (1.1), is that the AEB system demands full braking on all wheels while the ESC tries to stabilize the vehicle by braking individual wheels, visualized in Figure (1.2). In this case the brake ECU will have one signal from the AEB control algorithm to maximize the braking forces on all wheels and one signal to add braking force on individual wheels from the ESC algorithm. From this it is fairly easy to understand that it will be difficult for such a low level ECU, as the Brake module is, to make optimal decisions only based on requested brake torques or forces from different systems without knowing the reason why the systems are demanding what they are demanding.

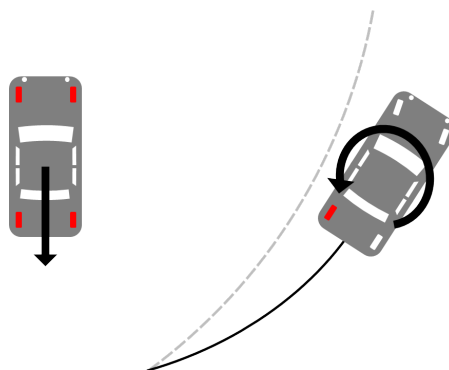


Figure 1.2: *The AEB system demands full braking on all four wheels to reduce the longitudinal speed as much as possible while the ESC system demands differential braking to create a yaw moment in order to remain stable and follow the intended path*

The structure of an integrated motion controller for an ADAS and for an autonomous system may differ. As an ADAS, the controller serves as a driver aiding system and shall therefore not behave contradictory to the driver intention. However, in a severe situation, an integrated motion controller could serve other purposes rather than to follow the expected behavior from the driver perspective to avoid a collision. Future autonomous vehicles using an integrated motion controller, based on internal vehicle sensors or information from the infrastructure, could add additional geometrical paths for evaluation with respect to given information regarding the surroundings etc. Thus, delay an intervention until only one path is possible giving a more robust, less occupant intrusive and safer vehicle. The possibilities for an implementation of an integrated motion controller in a future vehicle can therefore bring smarter and safer vehicles.

### 1.3 Objective

The objective of the thesis is to perform a motion analysis for future applications and requirements for road vehicles, as a step towards integrated control of the vehicle motion. A driving scenario of decelerating while cornering was chosen. The scenario can be divided into two contradictory motions; longitudinal deceleration, to decrease the speed of the vehicle to avoid or mitigate an imminent forward collision, and path following. The objective of the thesis involves an investigation of the motion in the scenario and a possible implementation of the results in an integrated brake controller. Within the objective of the thesis lies an investigation of the limitation of the scenario in terms of the benefits in using the full lane width during the intervention.

### 1.4 Delimitation

The vehicle motions of interest in the investigation was the planar dynamics (longitudinal, lateral & yaw). The vehicle model used in the investigation was a two track model with load transfer but with suspension effects suppressed. The scenario was evaluated with pseudo spectral collocation method via the optimal control package *PROPT*, through simulations in *Matlab/Simulink* for evaluating vehicle motion. The simulation model only used conceptual control e.g. braking forces was demanded from the wheels and a steer angle was determined from the wheels on the front axle. No detailed modelling of the driveline was being executed in the project and no rolling wheels has been used in the conducted simulations. In the optimizations performed, the road friction was always homogeneous i.e. split  $\mu$  or sudden changes of friction was not investigated. In the controller that was evaluated, this notion of constant friction is assumed to be known by the controller.

## 2 Vehicle Modeling

This section includes a brief explanation of the vehicle coordinate system and nomenclature used in order to express directions and rotations. The following section is also describing the modelling of a vehicle including equations of motion, the vertical load distribution due to longitudinal and lateral accelerations. The vehicle model represents a passenger vehicle with the ability to control each wheel brake force individually to meet the desired force demand.

### 2.1 Coordinate System

The coordinate system and nomenclature used in the report is seen in Figure (2.1).

- An inertial reference frame  $XYZ$ , defined as the global reference frame.
- A vehicle fixed frame  $xyz$ , defined as a body fixed coordinate system, with its origin,  $O$  at the center of gravity  $CoG$ .
- The rotation of the body fixed coordinate system relative the inertial reference frame is defined by the *roll*, *pitch* and *yaw* angles. Where *roll* defines the rotation around the  $x$ -axis, *pitch* as rotation around the  $y$ -axis and *yaw* rotation around the  $z$ -axis
- Positive direction of the body fixed  $x$ -axis is defined through the front of the vehicle. Motion along the  $x$ -axis is denoted as *longitudinal* motion.
- Positive direction of the body fixed  $y$ -axis is defined to the left, seeing the vehicle from above. Motion along the  $y$ -axis is denoted as *lateral* motion.
- Positive direction of the body fixed  $z$ -axis is defined through the vehicle roof. Motion along the  $z$ -axis is denoted as *vertical* motion.

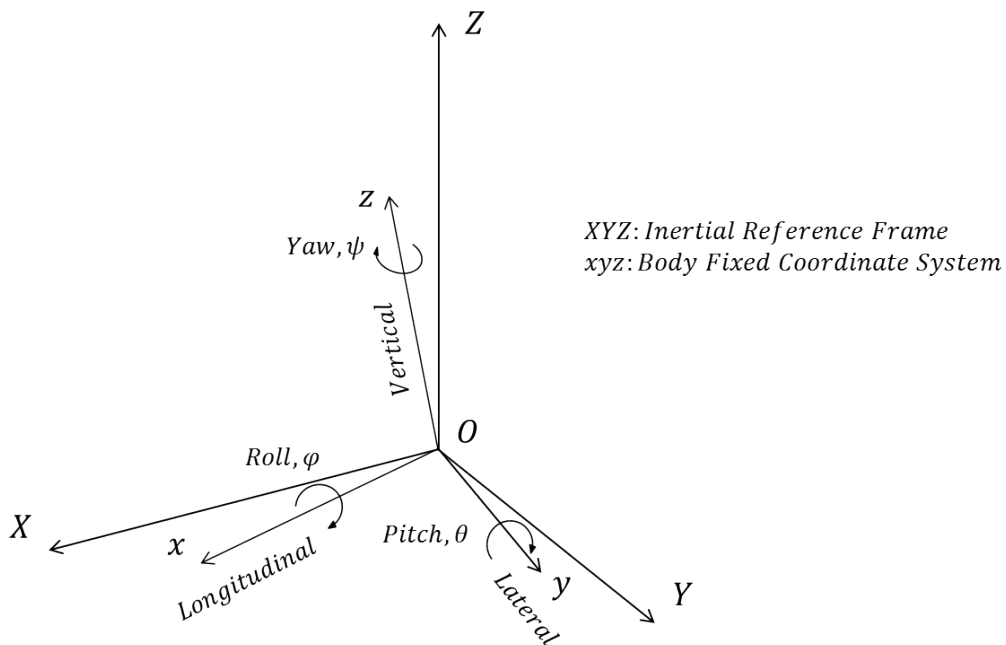


Figure 2.1: Coordinate system used throughout the report.

## 2.2 Two Track Model

The two track model is visualized in Figure (2.2). The vehicle model is a planar vehicle model where the equations of motions is derived through standard Newton-Euler theory. The vehicle model was derived in the body fixed reference frame explained in Section (2.1).

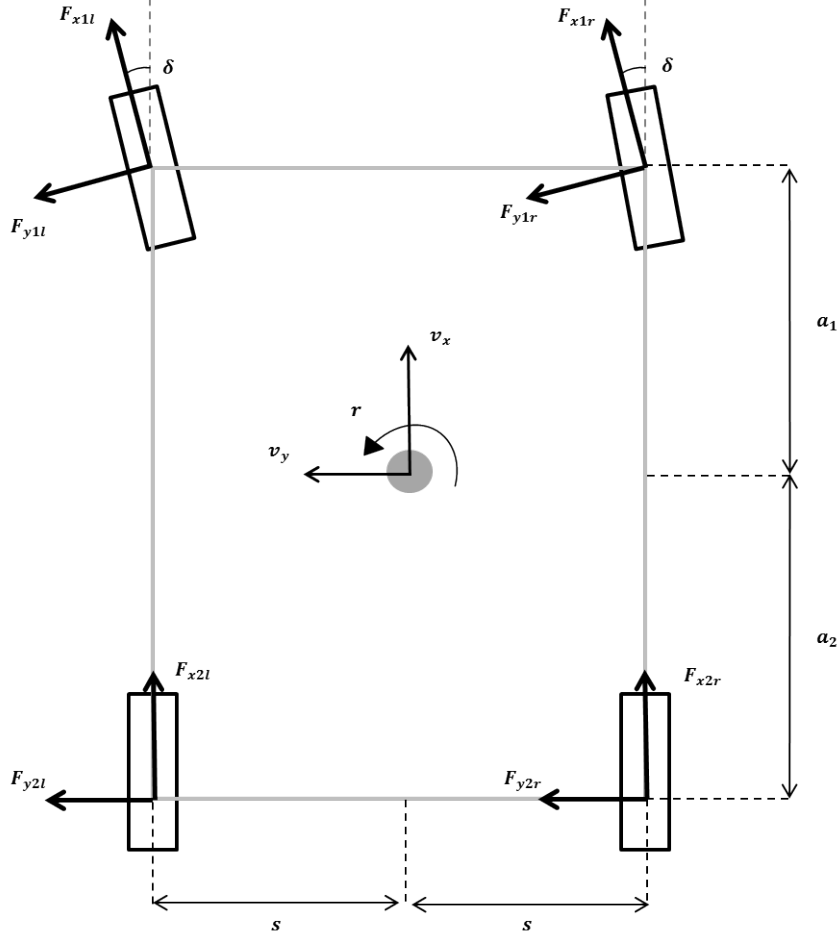


Figure 2.2: Freebody diagram for a two track model

The equations of motions, derived from the two track model can be seen in Expression (2.1) to (2.3). The steer angle of the left and right front wheel is assumed to be equal, i.e.  $\delta_{fl} = \delta_{fr} = \delta$ .

$$\sum F_x : (F_{x1l} + F_{x1r}) \cos \delta - (F_{y1l} + F_{y1r}) \sin \delta + F_{2lx} + F_{2rx} = m(\dot{v}_x - rv) \quad (2.1)$$

$$\sum F_y : (F_{y1l} + F_{y1r}) \cos \delta + (F_{x1l} + F_{x1r}) \sin \delta + F_{y2l} + F_{y2r} = m(\dot{v}_y + ru) \quad (2.2)$$

$$\sum M_z : ((F_{y1l} + F_{y1r}) \cos \delta + (F_{x1l} + F_{x1r}) \sin \delta) \cdot a_1 - (F_{y2l} + F_{y2r}) \cdot a_2 + (F_{x2r} + F_{x1r} \cos \delta + F_{y1l} \sin \delta) \cdot s - (F_{x2l} + F_{y1r} \sin \delta + F_{x1l} \cos \delta) \cdot s = J\dot{r} \quad (2.3)$$

$F_{xij}$  are the longitudinal forces and  $F_{yij}$  are the lateral forces acting on the vehicle with mass  $m$  and moment of inertia  $J$ . The moment of inertia is further described as  $J = mk^2$ , where  $k$  represents the radius of gyration. A real vehicle experiences load transfer due to longitudinal and lateral accelerations. The load transfer is highly

affecting the vehicle dynamics due to the non-linearity of the tires. The planar vehicle model used in this thesis is considering load transfer but with suppressed suspension effects. The static load distribution for each wheel is obtained by assuming a fully symmetric vehicle and is shown in Expression (2.4).

$$F_{zij} = \frac{m(L - a_i)}{2L}g \quad i = 1, 2 \text{ and } j = l, r \quad (2.4)$$

$a_i$  corresponds to the distance from the center of gravity to the front ( $a_1$ ) and rear ( $a_2$ ) axle. When the vehicle is accelerating or decelerating, the vehicle will experience a pitch motion. A constant longitudinal acceleration or deceleration of the vehicle gives that the pitch velocity and acceleration is zero which leads to only kinematic load transfer, seen in Expression (2.5).

$$\Delta F_{zx,i} = \frac{mh}{2L}a_x \quad (2.5)$$

$h$  and  $L$  are geometrical measurements corresponding to the center of gravity height and the total distance between the front and rear axle respectively. Similar to the pitch motion, the vehicle experience a lateral load transfer when cornering. Assuming that the vehicle is symmetric. i.e. center of gravity is in the middle of the track width. The expression for the lateral load transfer is seen in Expression (2.6).

$$\Delta F_{zy,i} = \frac{1}{2s_i} \left( \frac{c_{\varphi_i} h'}{c_{\varphi_1} + c_{\varphi_2} - mh'g} + \frac{(L - a_i)h_i}{L} \right) ma_y \quad (2.6)$$

The variable  $c_{\varphi_i}$  corresponds to the roll stiffness on each axle and  $h'$  represents a geometrical distance from the center of gravity to the roll axis defined through the roll center at each axle, described by  $h_i$ . A lateral load transfer coefficient,  $\zeta_i$ , describing the lateral load transfer that combines the roll stiffness distribution and the load transfer due to roll center height was introduced. The value of the lumped lateral load transfer coefficient is found in Appendix (A). The vertical force of the vehicle model is described by superposition of static load distribution and load transfer, assuming quasi steady state conditions. The vertical load for each tire is displayed in Expression (2.7).

$$F_{zij} = \frac{m(L - a_i)}{2L}g \pm \frac{mh}{2L}a_x \pm \zeta_i ma_y \quad (2.7)$$

$$i = 1, 2 \text{ and } j = l, r$$

The vehicle environment is simplified and external forces are neglected, i.e. the vehicle model does not take aerodynamic or rolling resistance into account. The vehicle data and parameters are listed in Appendix (A) and Appendix (B) together with a more detailed explanation of the vertical load transfer.

## 2.2.1 Tire Modelling

The lateral slip, defined as the slip angle  $\alpha_{ij}$ , determines the lateral forces of the wheels. It is derived from the steer angle and the velocities, experienced on each wheel. The lateral slip is further described as the lateral velocity divided by the longitudinal velocity at each wheel. For any given wheel the equation for the slip angle,  $\alpha_{ij}$ , becomes:

$$\alpha_{ij} = \delta_i - \arctan \left( \frac{v_{yij}}{v_{xij}} \right) \quad i = 1, 2 \text{ and } j = l, r \quad (2.8)$$

A more detailed derivation of the slip angles can be found in Appendix (B). The amount of longitudinal and lateral force on the wheels can be simplified as a function of the amount of the slip components together with the amount of vertical force and the friction coefficient in the contact patch. The dynamics of tires

are however more advanced and it shows a non-linear relation to the slip angle which can be seen in Figure (2.3)[15]. The figure also displays the effect of combined slip i.e. how longitudinal and lateral slip affects the amount of longitudinal and lateral force the tires can produce defined by the total budget of road adhesion. The longitudinal and lateral force is utilizing the same budget of road adhesion, which can be seen in the side force versus brake force diagram.

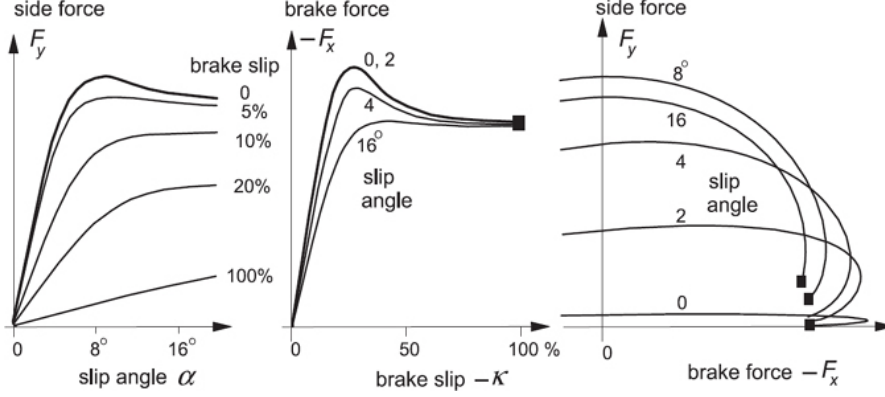


Figure 2.3: The tires shows a non-linear degressive behavior. Figure from [15].

From Figure (2.3) it can be concluded that the tire can not produce a larger force after a certain point of slip, i.e. the tire saturates. The behavior of the tires differs between tire to tire, however a common characteristics of saturation can be identified. The modeling of the tire behavior and the non-linearity of the tires is therefore a complex, also considering that different tires behave differently. A simplified tire model is shown in Expression (2.9). This tire model captures the saturation of the tires but is not load degressive and has no distinct peak in lateral force. The simplified tire model is well suited for optimization, since a hyperbolic tangent function saturates and converges to a certain value.

$$F_{yij} = D_{yij} \cdot \tanh(C \cdot B \cdot \alpha_{ij}) \quad i = 1, 2 \text{ and } j = l, r \quad (2.9)$$

The letter  $D_{ij}$  represents the peak value i.e.  $D_{ij} = \mu F_{zij}$  if pure lateral forces are considered. The peak value  $D_{ij}$  was expressed using simple combined slip model assuming the longitudinal forces as known, seen in Expression (2.10).

$$D_{yij} = \sqrt{(\mu F_{zij})^2 - F_{xij}^2} \quad i = 1, 2 \text{ and } j = l, r \quad (2.10)$$

Where the longitudinal force is within the range  $\mu F_{zij} \cos(\alpha) \leq F_{xij} \leq \mu F_{zij}$ . The tire behaviour can be modelled as linear when operating in the region of small slip angles. The slope of the linear tire region is named cornering stiffness,  $C_{F\alpha}$ . The cornering stiffness is therefore defined by  $C_{F\alpha} = \left. \frac{dF_{yi}}{d\alpha_i} \right|_{\alpha_i=0} = BCD$ .

### 3 Decelerating in a Curve

To evaluate vehicle motion priority, a scenario where vehicle motions are contradictory was investigated. The scenario of decelerating while cornering was selected, with the contradictions being to decelerate as much as possible while controlling path deviation. The damping of yaw motion is decreased with increased vehicle speed. Thus, stability of the vehicle must be considered when cornering. Conditions for a proper braking intervention is therefore not only focused on decreasing the braking distance but also on performing the maneuver in a safe fashion [16]. Yaw stability is therefore of equal interest as the braking distance [16].

The number of possible variations of a deceleration in corner scenario is limitless which prompted a simplification and parameterization of the scenario. The parametrization was done to objectify the scenario and the results. This parametrization can be seen in Figure (3.1). The braking distance,  $d_b$ , was defined as the travelled arc length along the reference circle,  $R_0\varphi$ , during the time history  $t = 0$  to  $t = t_f$ . To parametrize the objective of path following, off-tracking  $d_{off}$ , was defined. This was defined as the increase in radius from the origin of the reference circle.

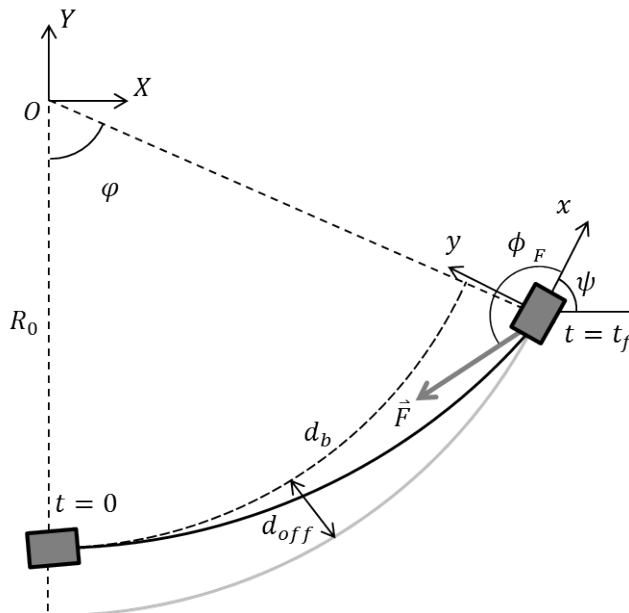


Figure 3.1: *Parametrization of the driving scenario.*

The theoretical velocity limit for following a curve with a specified path curvature and the available combined friction of  $\mu$  can be seen in Expression (3.1).

$$v_{lim} = \sqrt{v_x^2 + v_y^2} = \sqrt{\mu g |\kappa^{-1}|} \quad (3.1)$$

Real-world driving involves braking in large curve radii. Motorway corners are designed with curve radii above 800 m, motorway intersections and merging points are designed with radii between 300 and 900 m. Normal roads usually have curve radii above 200 m [16]. However, in overtaking situations, the curve radius can be decreased to lower figures which motivates the use of a smaller curve radius than used for infrastructure design. In the case of a curvature of  $|\kappa_0^{-1}| = R_0 = 150$  m and a friction coefficient of  $\mu = 1$  the maximum velocity is calculated to  $v_{lim} = 138$  km/h. A vehicle that experience an initial velocity  $v_0$  larger than the limit velocity  $v_{lim}$  will therefore deviate from the intended path and a terminal understeer situation will be caused [17]. In the scenario evaluated in this thesis, defined as deceleration in a corner, the brakes are assumed to be applied in the corner for a non-overspeeding situation, i.e.  $v_0 < v_{lim}$ . The applied braking is therefore the reason for inducing a possible path deviation. This scenario has been investigated using the method of optimal control which is introduced below.

### 3.1 Optimal Control Preliminaries

Optimal control is the theory of how to find the optimal way of controlling a dynamic system between two boundary states. The field emerged and developed through the cold war because of the need to solve flight path optimization problems for fighter aircraft. Big contributions came from the Russian mathematician Pontryagin [18]. Among other things he formulated the Pontryagin Principle which is a necessity to be sure of optimality conditions. The optimal control problem has an objective of minimizing or maximizing a cost function. This cost function can include both end objectives as well as objectives integrated over the whole control phase. A numerical method for solving optimal control problems is by using a Pseudo-Spectral Collocation Method. This is the method used in the thesis and it discretizes and turns the problem into a nonlinear program. A nonlinear program is an optimization problem subject to constraints where any of the functions are nonlinear [19]. The discretization is a collocation method where the states and controls are expressed as high-degree polynomials and are solved in all collocation points (discretization points). Constraint violations of the dynamic system can only be evaluated in the collocation points, meaning that there is no guarantee that the solution is valid between the collocation points. However, if increasing the number of collocation points and running the optimization again does not yield a different solution, the number of collocation points are sufficient. To solve these problems the optimal control package PROPT [20] for MATLAB has been used.

### 3.2 State of the Art Representation Using Fixed Brake Proportion with Optimal Steering Input

An evaluation of how a brake system of today handles in this situation has been done. The reference representation was designed so that it uses a fixed brake proportion with select low on the front axle. A front biased brake distribution of  $F_{x1}/F_{x2} = 90/10$  was used for the state of the art representation of a reference brake system. The braking force was determined from Expressions (3.2) and (3.3).

$$F_{x1l} = F_{x1r} = -\mu \cdot \min(F_{z1l}, F_{z1r})$$

$$i = 1, 2 \text{ and } j = l, r \quad (3.2)$$

$$F_{x2l} = F_{x2r} = \frac{10}{90} \cdot -\mu \cdot \min(F_{z1l}, F_{z1r})$$

$$i = 1, 2 \text{ and } j = l, r \quad (3.3)$$

The fixed brake distribution was chosen to be large (90% front) between front and rear axle to utilize much road adhesion on the front axle during the brake intervention, due to load transfer, without locking front or rear axle. A large acceleration was seen from start of the brake intervention which motivates a large front shifted brake distribution to utilize the front vertical force. A lower front shifted brake distribution showed wheel lock-up on the rear axle during the initial part of the scenario, explained by the large lateral load transfer at the beginning of the maneuver. A first reference system simulation was conducted with full braking according to Expression (3.2) and (3.3) with fixed steer angle named Fixed Brake Proportion (FBP). A second reference system simulation was conducted with optimal control of one brake input, mimicking the modulation of a brake pedal, together with optimal control of the steering. The reference utilizing select low together with a fixed brake distribution is representing a close to ideal, braking intervention with an optimal steer angle input from a driver or an Active Front Steer (AFS) system. This reference system can modulate the brake force during the maneuver. The steer input from the driver or an Active Front Steer (AFS) system represents the optimal modulation of the steer angle to keep the intended vehicle path. One can therefore see the second reference case as an optimal driver braking in the corner and was named Fixed Brake Proportion Steering (FBPS).

The braking distance for the reference system FBP and FBPS are displayed in Table (3.1) for the initial velocity of 90 km/h and 135 km/h for a corner radius of 150 m with an allowed off-tracking of 0.5 m.

Table 3.1: Braking distances for two different cases with an allowed off-tracking of 0.5 m

$d_{off} = 0.5$ m	90 km/h	135 km/h
FBP	41.9* m	100.1* m
FBPS	39.6 m	106.3 m

\* Deviates from the intended path.

The trajectories and the lane utilization for the case of 135 km/h, for the same corner radius and allowed off-tracking as discussed above, are shown in Figure (3.2) and (3.3).

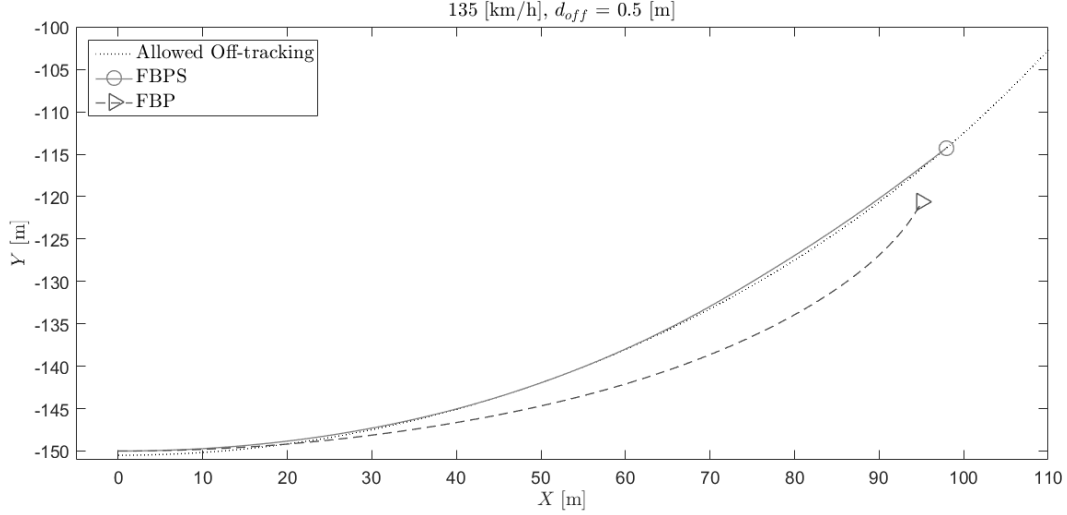


Figure 3.2: Trajectory lines for the two reference systems; (FBP) Fixed brake proportion and (FBPS) Fixed brake proportion with steering.

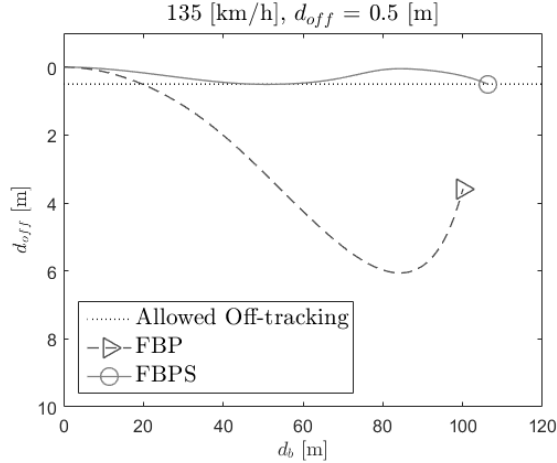


Figure 3.3: Off-tracking vs travelled distance for the two reference strategies.

From the braking distance, trajectory and off-tracking it can be concluded that the reference braking systems requires an optimal steer angle to stay within the allowed off-tracking (intended path). The braking distance for FBP showed a smaller braking distance compared to FBPS in the higher velocity case. This is however due to the large off-tracking received with a fixed steer angle seen in Figure (3.2) and (3.3). It was therefore concluded that the reference system with optimal controlled brakes, with a fixed brake proportioning, and optimal controlled steering is preferred as a reference system for later comparison. This since only using the

optimal modulation of the brakes yielded poor results. The reference with optimal braking, with a fixed brake proportioning, and optimal steering performs well regarding staying within the allowed off-tracking. However, this represents the optimal driver modulating both steering and brakes. This knowledge must be remembered later where results from only using the brakes are compared with this reference system which is the optimal driver modulating both brakes and steering.

### 3.3 Individual Wheel Braking with Optimal Control

The results from the reference systems shows that the scenario of braking in corner can be handled with a fixed brake proportion with optimal controlled steering. However, the true optimal solution without any limitations is wanted in the evaluation for future control applications. This section is therefore deriving the optimal control problem and investigating the results for the chosen scenario. The optimization has been performed with individual braking forces as the main actuator. However, adding optimal controlled steering has also been evaluated since the results where the steering is optimally controlled gives valuable insight the motion during the scenario. Optimal controlled steering has been left out in later analysis of the scenario and in controller design.

#### 3.3.1 Formulation of the Optimal Control Problem

The vehicle model shown in Chapter (2) and further explained in Appendix (B) was used for the optimization in PROPT. The formulation of the optimal control problem is described in this section. Firstly, the states and control variables of the system need to be introduced. The vehicle state vector consist of the global position, the heading angle, the velocities and yaw rate of the two track model seen in Expression (3.4).

$$x = [X \quad Y \quad \psi \quad u \quad v \quad r] \quad (3.4)$$

The longitudinal tire forces were used as the control inputs as seen in Equation (3.5).

$$u = [F_{x1l} \quad F_{x1r} \quad F_{x2l} \quad F_{x2r}] \quad (3.5)$$

To optimize the control in the scenario described above, the objective of maximizing deceleration is met through minimization of the stopping time  $t_f$ , seen in Equation (3.6), subject to the final boundary condition of the simulation, seen in Equation (3.7). The final boundary condition defines the stopping point of the simulation, in this case when the total velocity is approaching the velocity threshold  $v_{thr}$ , which was set close to zero.

$$J = t_f \quad (3.6)$$

$$v_x(t_f)^2 + v_y(t_f)^2 = v_{thr}^2 \quad (3.7)$$

The initial boundary condition, defined in Equation (3.8), and steer angle were derived from steady state cornering conditions. The steer angle corresponds to that of a slightly understeered vehicle. The initial position of the vehicle in the global reference frame was set so that the vehicle initiates the scenario in the bottom of a reference circle with its origin in the reference frame origin.

$$x(t_0) = [0 \quad -R_0 \quad \psi_0 \quad u_0 \quad v_0 \quad r_0] \quad (3.8)$$

The second scenario objective of an allowed off-tracking,  $d_{off}$ , was incorporated into the optimization as a barrier constraint on path deviation, according to Expression (3.9) [19]. The control inputs were also limited according to Expression (3.10) which represents a simple combined slip model.

$$(R_0 - d_{off})^2 \leq X^2 + Y^2 \leq (R_0 + d_{off})^2 \quad (3.9)$$

$$F_{zij}^2 = F_{xij}^2 + F_{yij}^2 \quad i = 1, 2 \text{ and } j = l, r \quad (3.10)$$

The optimization requires a proper initial guess of the states and controls of the simulation in order to find the optimal solution. The initial guess was derived from a particle representation of the same problem.

### 3.4 Analysis of Braking Strategies shows Transient Behaviour

Firstly, optimizations were run for the problem introduced in the section above. The initial optimal control results using the strategy of only braking showed excessive side slip angles, with maximum values in the range of  $60^\circ$ . A side slip constraint was therefore implemented. The implementation of this constraint into the optimization can be seen in Equation (3.11).

$$\tan^{-1}(\beta_{lim}) \cdot v_x \geq |v_y| \quad (3.11)$$

The non-constrained case of optimal braking was compared to the optimal braking with a side slip constraint of  $\beta_{lim} \leq 10^\circ$ . Although the side slip was decreased significantly, minor differences regarding braking distances were observed for the different test cases. The comparison can be seen in Table (3.2).

Table 3.2: *Minor effects was observed in braking distance comparing the optimal braking strategy with and without a constrained  $\beta(t)$  to maximum  $10^\circ$ . In this case the reference path radius was 150 m.*

$d_{off}$ m	0.05 m	0.5 m	1 m	2 m
90 km/h	34.41 <sup>a</sup> m	32.85 <sup>a</sup> m	32.33 <sup>a</sup> m	31.80 <sup>a</sup> m
	34.45 <sup>b</sup> m	32.87 <sup>b</sup> m	32.36 <sup>b</sup> m	31.81 <sup>b</sup> m
120 km/h	67.29 <sup>a</sup> m	63.92 <sup>a</sup> m	62.36 <sup>a</sup> m	60.43 <sup>a</sup> m
	67.47 <sup>b</sup> m	64.06 <sup>b</sup> m	62.52 <sup>b</sup> m	60.55 <sup>b</sup> m
135 km/h	97.31 <sup>a</sup> m	90.82 <sup>a</sup> m	87.65 <sup>a</sup> m	83.58 <sup>a</sup> m
	97.58 <sup>b</sup> m	91.01 <sup>b</sup> m	87.72 <sup>b</sup> m	83.63 <sup>b</sup> m

<sup>a</sup> *Optimal braking without side slip.*

<sup>b</sup> *Optimal braking with side slip constraint,  $\beta_{lim} \leq 10^\circ$ .*

The results showed that the braking distances were almost unchanged while side slip was greatly reduced. However, the time histories of the control inputs (the brake forces) showed large differences. Optimizations was further on performed with the side slip constraint implemented. This was done for two strategies. One being to only use the longitudinal tire forces as controls according to Expression (3.5). This is from here on called OCB (Optimal Control Braking). The other strategy did include the steering as an extra control input, with constraint according to Expression (3.12). This strategy is further on called OCBS (Optimal Control Braking & Steering).

$$|\delta_f| \leq \delta_{lim} \quad (3.12)$$

To analyze the differences that appear between the systems and the overall motions in the scenario, an analysis of the optimal results for the two strategies was done. The comparison of the OCB and OCBS gives valuable insight into the motion needed in order to minimize brake distance and staying on the intended path with a deviation equal to the allowed off-tracking. The optimization cases were done for a corner radius of 150 m with varying initial velocity and varying allowed off-tracking. A first comparison to do is to compare the trajectories of the systems which can be seen in Figure (3.4).

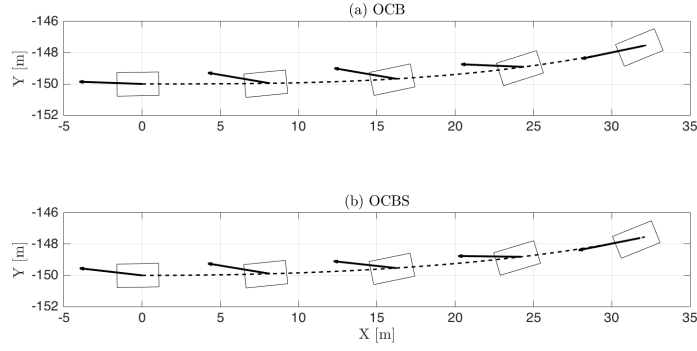


Figure 3.4: Trajectories for different strategies in the case of an initial speed of 90 km/h and an allowed off-tracking of 0.5 m. (a) OCB shows optimal braking solution with fixed steer angle, (b) OCBS represents the optimal braking together with optimal steering.

From the overall look of the trajectories, it can be seen that there are no large differences between the two strategies. The global force vector, shown by the arrows, in Figure (3.4) at different steps shows similarities as well. However, one difference can be observed. From the global angle of the force vectors, the OCB tend to allocate more of the grip for longitudinal braking compared to OCBS initially. By examining how the strategies make use of the allowed off-tracking, the overall motion priority and global forces of the scenario can be determined, this is depicted in Figure (3.5)

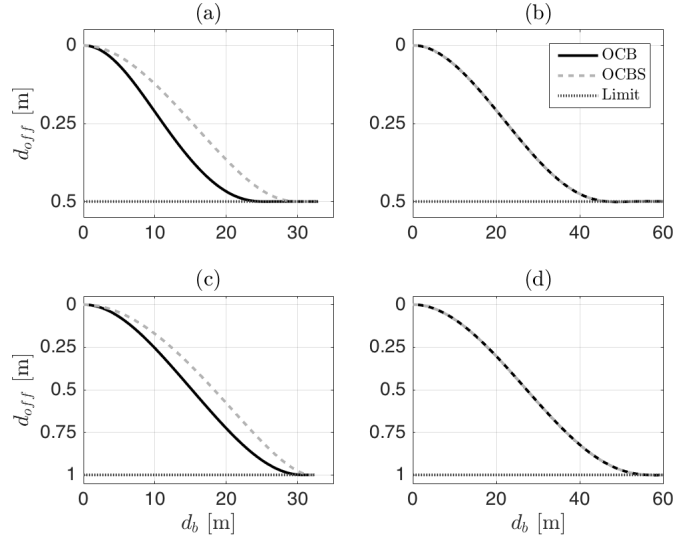


Figure 3.5: The deviation from the reference path plotted against the travelled distance. (a & c) has initial speed of 90 km/h and (b & d) has the initial speed of 135 km/h with a corner radius of 150 m. The allowed off-tracking for the cases are depicted as the dotted line "Limit".

From Figure (3.5) the differences between the strategies are more pronounced. For the case of a lower initial speed (90 km/h), it can be seen that by introducing steering as a control (OCBS) the solution tends to reach the limit of off-tracking later into the scenario. In the case of an initial speed of 135 km/h this difference is not noticeable and both models are very similar in results. The reason for this earlier path deviation by the OCB shows that it does not allocate as much grip as the other strategy for lateral acceleration in the beginning of the maneuver. To analyze this difference, the global acceleration utilization is depicted in Figure (3.6). The

maximum possible acceleration is defined by the road friction and the gravity constant, i.e.  $\mu g$ .

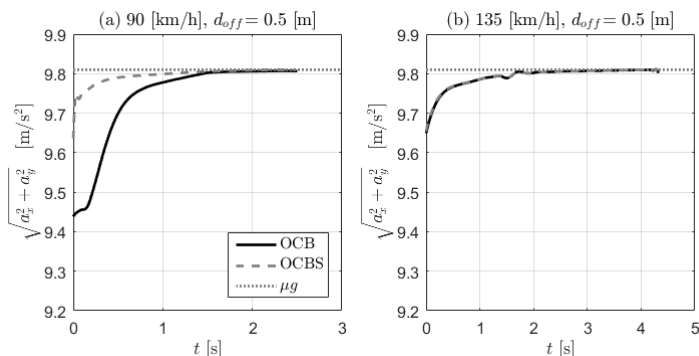


Figure 3.6: (a & b) shows the resultant acceleration for the case of 90 and 135 km/h for the OCB and OCBS.

Figure (3.6) shows that the optimal solution builds up the acceleration magnitude during the initial part of the braking maneuver, for both OCB and OCBS. The reason for a slower acceleration magnitude buildup for OCB is explained by the lack of sufficient lateral forces initially. This can be further explained by that the lateral forces of the two track model is dependent on lateral slip. However, there is a possibly internal forces used for rotation of the vehicle which cancels out when studying the global acceleration. Instead it would be of interest to investigating the yaw moments for each optimal case. Figure (3.7) displays the time history of yaw moment acting on the vehicle for OCB and OCBS for the cases an initial velocity of 90 and 135 km/h and an allowed off-tracking of 0.5 m.

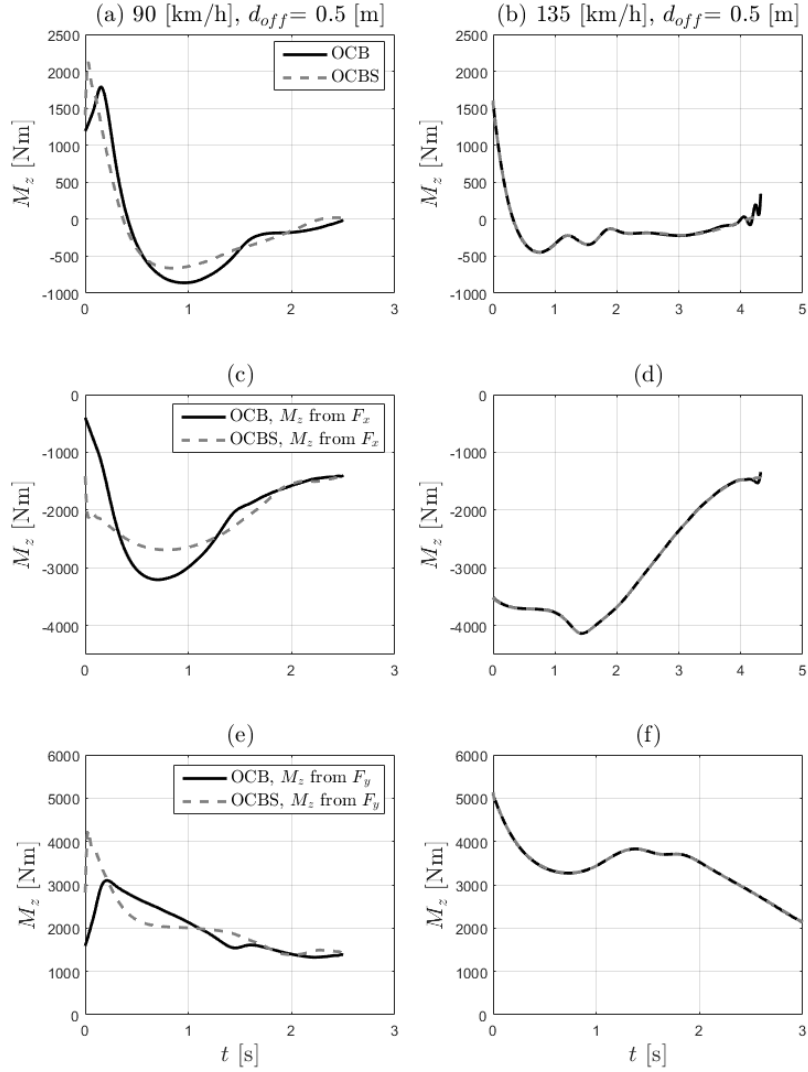


Figure 3.7: *Left column show yaw moments for 90 km/h while right column show yaw moments for 135 km/h. (a & b) Total yaw moment, (c & d) Longitudinal contribution to yaw moment, (e & f) Lateral contribution to yaw moment.*

Figure (3.7 a & b) shows the total yaw moment of the vehicle which coincides fairly well for the two strategies, although tends to coincide better for higher velocity. A difference can be observed for the yaw moments brought to the vehicle from the longitudinal and lateral forces seen in Figure (3.7 c & d) and (3.7 e & f), respectively. The yaw moments caused by longitudinal forces are negative during the entire maneuver, corresponding to a turn out moment i.e. the braking forces alone creates a moment that would make the vehicle rotate outwards in the corner defined as a left turn. The turn out moment from the longitudinal forces corresponds to a larger longitudinal forces on the outer wheels (FRW and RRW). A similar turn out moment has shown to be advantageously for limiting deviations from a reference path [17]. The magnitude of turn out moment from the braking forces differs between the optimal braking and the optimal braking with optimal steering. The OCB tends to have a lower amount of turn out moment initially compared to the OCBS, which is explained by the lack of lateral turn in moment caused by lateral forces. The lateral turn in moment is of lower magnitude initially. This is the reason for the increased braking distance compared to OCBS, because the longitudinal force cannot be applied fully on the outer wheels without leaving the intended reference path. When the

vehicle experience a corner situation a higher vertical load is naturally seen on the outer wheels. The lack of turn out moment in OCB indicates that less of the vertical force can be utilized on the outer wheels, thus a lower longitudinal acceleration is achieved. The acceleration level and the yaw moment of the vehicle together provides information describing that OCBS can allocate more road adhesion to longitudinal forces since the lateral forces is large enough to counteract the turn out moment, provided by full longitudinal braking on the outer wheels. The larger turn in moment seen in OCBS provides information of that the steer angle can be used in order to decrease the longitudinal braking distance. Further analysis of the vehicle behavior is done by observing the yaw rate for OCB and OCBS, seen in Figure (3.8).

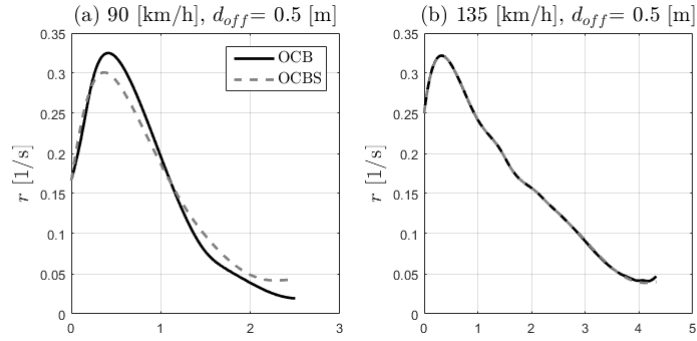


Figure 3.8: (a) Yaw rate for 90 km/h for an allowed off-tracking of 0.5 m, (b) Yaw rate for 135 km/h for an allowed off-tracking of 0.5 m.

A larger peak in yaw rate was observed for the case of fixed steer angle (OCB) compared to the non-fixed steer angle (OCBS) for the lower velocity case and coincides well for higher speeds. The initial yaw rate at  $t = 0$  s corresponds to the steady state yaw rate for the initial velocity and curve radius and is thereafter increasing. The increase in yaw rate is explained by that a certain rotation of the vehicle is needed to stay within the allowed off-tracking and at the same time utilize braking on outer wheels. Braking on outer wheels creates a turn out moment, which decrease the yaw rate during the maneuver. This can be further analyzed by observing the actual and effective curve radius of the vehicle model in Figure (3.9) for the lower velocity case of 90 km/h. An effective curve radius is calculated by the Expression (3.13) and is compared to the actual curve radius, defined in Appendix (B), which is the actual curvature of the path that the vehicle has travelled.

$$\kappa^{-1} = \frac{v_x}{r} \quad (3.13)$$

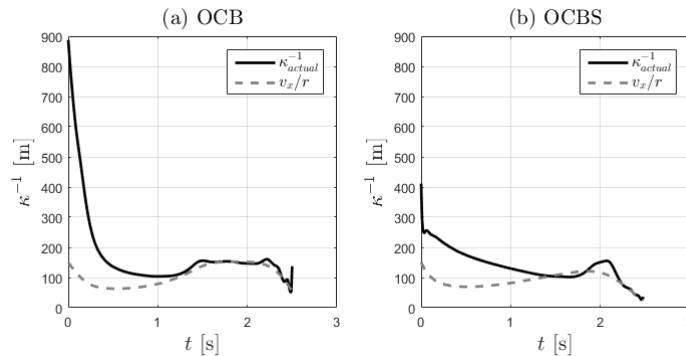


Figure 3.9: Effective and actual curve radius for 90 km/h for an allowed off-tracking of 0.5 m for (a) OCB and (b) OCBS.

From the Figure (3.9) difference can be observed in the first part of the maneuver, comparing the actual curve radius determined from the vehicle path and the effective curve radius. A larger difference can be observed in the fixed steer angle case (OCB), showed in Figure (3.9a), therefore it can be concluded that the yaw

rate increase initial in the scenario is provided to rotate the vehicle rather than following the actual path curvature. The rotation of the vehicle can be explained by the need of maximizing the available lateral forces to counteract the turn out moment from the longitudinal brake forces. A smaller difference between the curvature measurements was observed for the higher speed cases. The difference can be found in that the optimal control with steering (OCBS) can add steering wheel angle which produces the desired slip angles. This can be seen in Figure (3.10) where the steering wheel angles are compared between the strategies as well as the mean front axle slip angle.

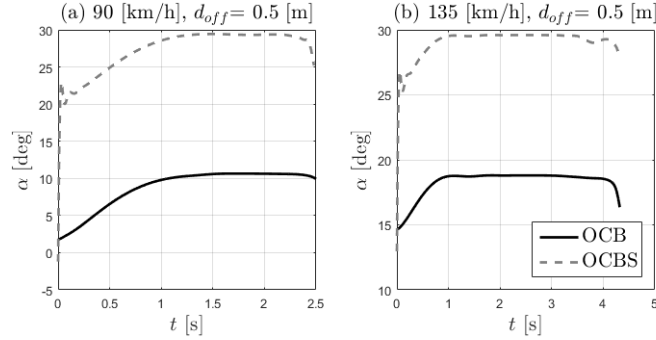


Figure 3.10: The front wheels slip angles for the cases, (a) 90 and (b) 135 km/h with an allowed off-tracking of 0.5 m.

High slip angle levels are observed in Figure (3.10) for case of optimal controlled steer angle (OCBS), caused by the use of a large, unrealistic, steer angle. The optimal steer angle over the time history showed that the magnitude of the steer angle should be kept high during the maneuver. The result was consistent for all conducted optimizations and indicates that having large slip angles guarantees that the lateral forces will be large if the grip is not used for longitudinal forces. Figure (3.11) shows both the absolute values of the braking forces as well as the normalized braking forces with respect to vertical load for the OCB solution.

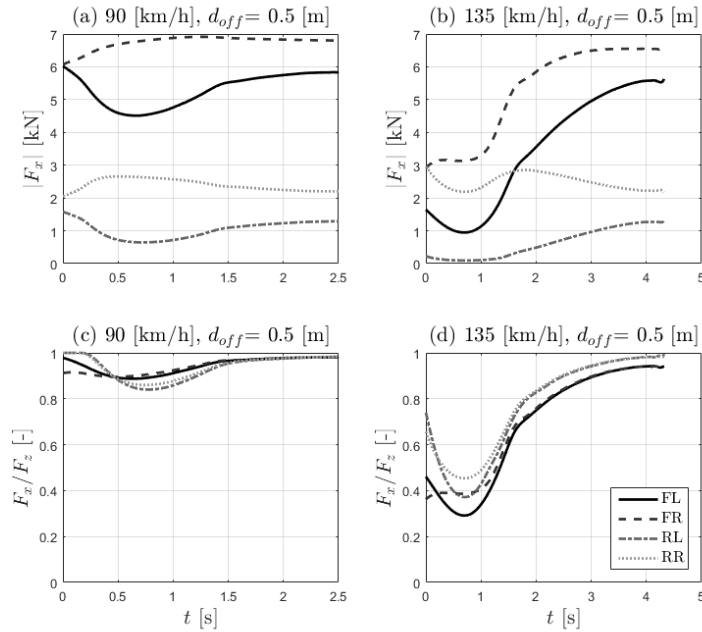


Figure 3.11: (a & b) shows the absolute braking forces while (c & d) shows the normalized braking forces. (a & c) and (b & d) is the cases with an initial speed of 90 km/h and 135 km/h, respectively.

What can be seen from Figure (3.11) is that there are two distinct phases of the maneuver. Initially, there is a phase where the normalized forces show a transient behavior in right/left proportion, originating from a desired yaw moment on the vehicle. It can be observed that after this initial phase the normalized brake forces on the front axle are very similar which also is true for the two rear tires. At higher speeds, in the case of an initial speed of 135 km/h the rear axle allocates a higher proportion of the available friction for longitudinal braking compared to the front axle, i.e. the rear axle is closer to a possible lock up. This differs from systems used today where grip on the rear axle is wanted to prevent skidding and a potential unstable maneuver.

Further analysis of the transient yaw motion can be done by observing the time history of the force vector angle. The two distinct phases are also seen in Figure (3.12), where the transition between the phases is visualized clearly. The force vector angle describes the direction of the sum of all planar forces acting on the vehicle where  $90^\circ$  represents full lateral usage and  $180^\circ$  indicates full longitudinal deceleration.

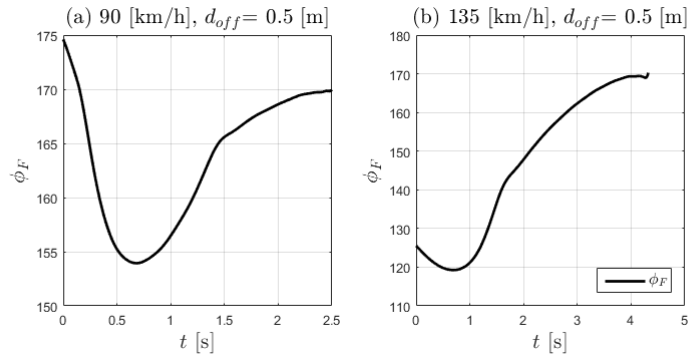


Figure 3.12: (a) Shows the force vector angle for the case of 90 km/h for an allowed off-tracking 0.5 m. (b) shows the force vector angle for the case of 135 km/h for an allowed off-tracking 0.5 m with OCB strategy.

It can be seen that when only using the optimal brakes with fixed steer angle (OCB), there is a need to generate the slip angles by rotation of the vehicle using the braking forces. When an optimal steering is introduced this lateral force is generated from a larger steer angle. The same reasoning can be applied to explain that the OCB and OCBS coincide well at higher speeds where the lateral force is present earlier into the maneuver. Due to the higher initial lateral acceleration in the 135 km/h case, the yaw rate and lateral velocity is already sufficiently large. This means that without steering, it is still possible to generate large lateral tire forces that counteracts the turn out moment from the longitudinal forces. From the analysis of the yaw rate, yaw moment, slip angles and the braking forces for the optimal control results it can be concluded that the transient behavior is developing because the vehicle needs additional side slip to ensure full utilization of the available lateral force. This can be concluded from observing the differences of the two strategies since the transient phase is shorter when using steering since the desired lateral forces can be obtained earlier by turning the wheels than by rotating the whole vehicle as in OCB. The transient is also explained by the fact that the initial condition of the vehicle is based on the constant velocity in steady state cornering, however when the brakes are applied the constant speed steady state is changed and a transient behavior is observed until quasi-steady state in the braking maneuver is reached. The transient behavior indicates that the constant speed steady state conditions initially experiences a lower lateral acceleration and a need of rotating the vehicle to keep to the optimal path.

Development of a future controller cannot control the vehicle based on this transient behavior. As stated previously, the braking distance and the stability during the maneuver is of equal interest. A brake controller that brakes with a set point of rotating the vehicle initially can therefore cause instability rather than mitigating such a motion. This could also make the controller sensitive to disturbance, like road adhesion changes, road irregularities etc., which causes an opposite effect compared to a robust brake controller. However, a future brake controller based on the second distinct phase could be utilized and can therefore operate during quasi-steady state deceleration. Quasi-steady state means that the vehicle is in a phase when braking already has been initiated, and jerks are small i.e. accelerations are changing slowly.

### 3.5 Neglecting the Transient Phase Yields Quasi-Steady State Solution

The main observation from the analysis in the previous section was that this transient buildup of side slip is highly dynamic, and that the investigation should focus on the quasi-steady phase that was observed in previous sections. The quasi-steady phase implies that acceleration changes are small and that the braking has already been initiated. From real vehicle braking it is known that the brake forces cannot be applied fully at an instant. The transient behavior occurred due to the fact the a step braking was applied when the vehicle was in a constant speed steady state condition, where the lateral acceleration magnitude initially was lower than during the quasi-steady state braking intervention. Given the analysis above it was decided to solve the optimal control problem with the OCB system but altering the initial boundary conditions. This was done to capture the quasi-steady state behavior while removing the highly dynamic transient behavior, similar to applying the brakes with a ramp, to capture the real vehicle behavior where the brake force are built up during a short time and is not applied as a step. This meant that Expression (3.8) was removed and replaced by Expression (3.14). It was used to make sure that the initial velocity vector angle would be correct in the inertial reference frame while still keeping the initial heading angle of the vehicle as a free boundary. A boundary condition of the total velocity equal to the initial speed of the vehicle was set.

$$\begin{aligned}
 x_1(t_0) &= 0 \\
 x_2(t_0) &= -R_0 \\
 v_x(t_0) &= V_0 \cos \psi \\
 v_y(t_0) &= -V_0 \sin \psi \\
 V_0^2 &= v_x(t_0)^2 + v_y(t_0)^2
 \end{aligned} \tag{3.14}$$

This boundary condition limits the vehicle position to coincide with earlier optimization. The initial velocities are also constrained so that the vehicle is travelling along the reference circle but with a free heading angle and yaw rate. The solution could therefore increase the lateral velocity with an upper limit based the imposed side slip constraint. The free boundary conditions is therefore increasing the magnitude of the lateral velocity and lateral acceleration to simulate that quasi-steady state braking is reached from  $t = 0$ . Higher slip angles on the four wheels would therefore produce a larger turn in moment, thus decrease the transient behavior of rotating the vehicle in the initial part of the brake maneuver. This due to that the initial rotation is already accounted for when observing the quasi-steady state part of the maneuver. This can be seen by observing the yaw moment for the quasi-steady solution with an allowed off-tracking of 0.05 and 0.5 m, seen in Figure (3.13).

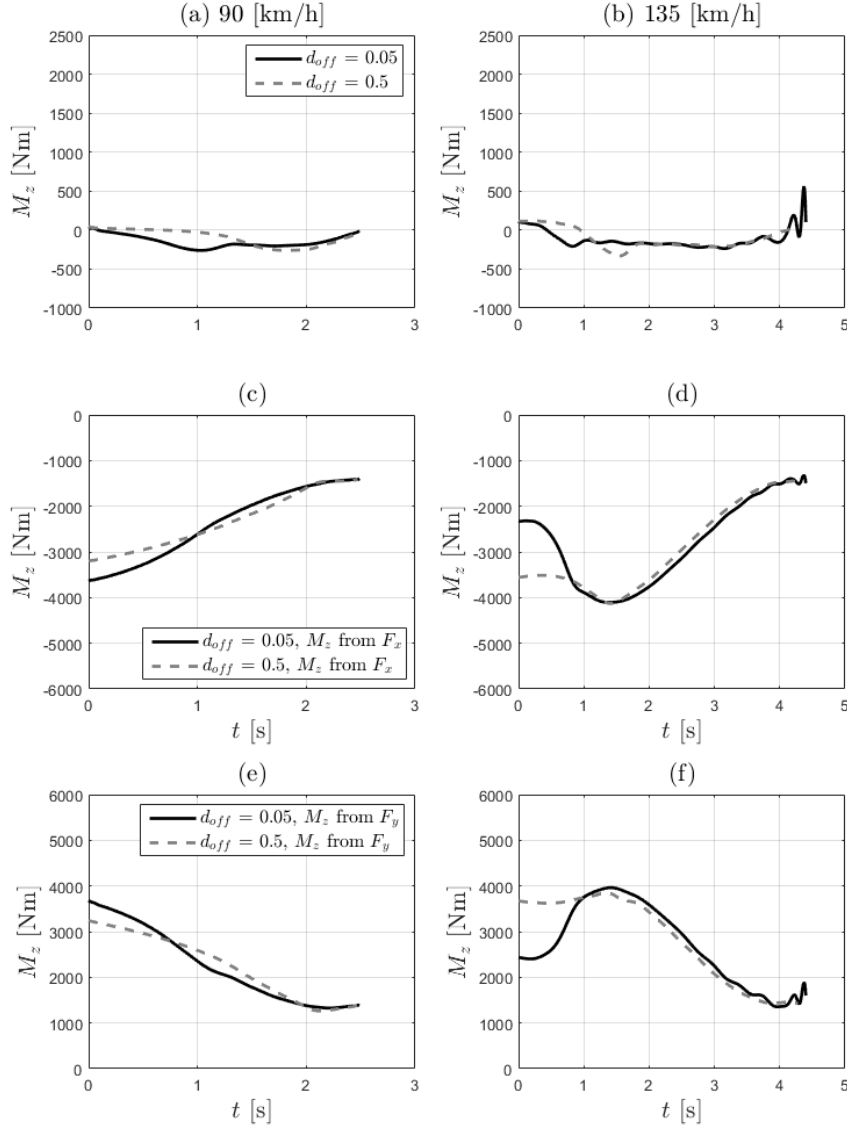


Figure 3.13: Yaw moment comparison for quasi-steady braking for two values of allowed off-tracking and two different initial velocities. (a & b) shows total yaw moment, (c & d) shows yaw moment generated from longitudinal tire forces and (e & f) shows yaw moment from lateral forces.

The magnitude of the moment generated from the longitudinal force, seen in Figure (3.13 c & d), is increased initially compared to the previous case of an initial boundary of steady state cornering depicted in Figure (3.7 c & d). This can be explained by the increased magnitude of the lateral turn in moment which counteracts the increased braking force. The total yaw moment reaches small values, which indicates that a large proportion of the combined road adhesion is utilized for the purpose of maximizing longitudinal braking. It can therefore be concluded that the lateral force build up is of major importance for maximizing the longitudinal deceleration. The comparison of yaw moment between allowing an off-tracking of 0.05 and 0.5 m shows a difference. The smaller allowed off-tracking case shows a larger negative magnitude of yaw moment during the scenario, which indicates that less of the available road adhesion, is allocated to deceleration of the vehicle. Thus, an increased braking distance is expected. The vehicle states can be observed in Figure (3.14).

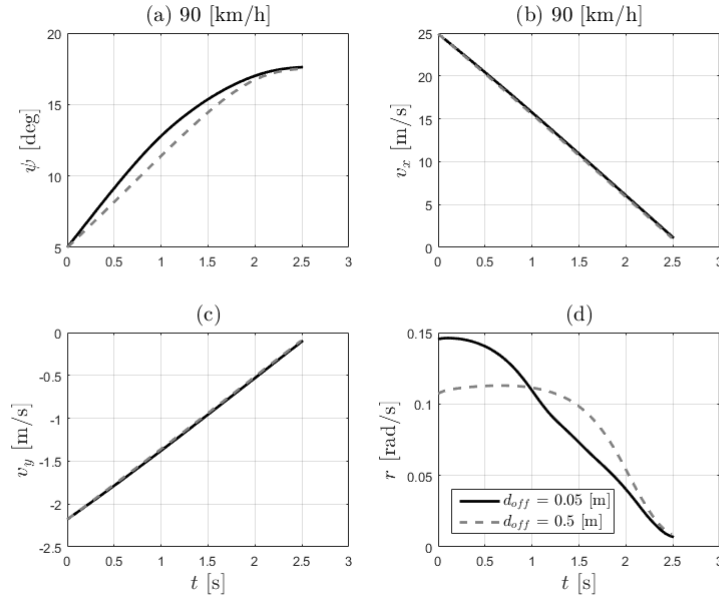


Figure 3.14: Vehicle states for quasi steady braking maneuver with imposed side slip constraint of  $\beta_{lim} = 10^\circ$  for an initial speed of 90 km/h in corner radius of 150 m. (a) heading angle, (b) longitudinal velocity, (c) lateral velocity and (d) yaw rate. The state time histories are derived through the strategy of OCB.

The most strict path constraint of 0.05 m shows that a larger yaw rate is wanted initially compared to the case of 0.5 m due to the need of following a more strict path constraint. The difference between the steady state cornering and the quasi-steady state braking is seen in the time history of the yaw rate. When free boundary conditions was applied, a proper initial yaw rate is provided, giving a lower yaw moment magnitude, i.e. in the quasi-steady case, the yaw rate is already at a sufficient level for following the actual path and less lateral force build up is needed. Comparing the case of an allowed off-tracking of 0.05 and 0.5 m, one can see a that a higher yaw rate is experienced initially for strict path following, which enables a higher turn out moment from the longitudinal force to keep the intended path. The quasi-steady state braking is therefore giving a too large initial yaw rate to ensure that the lateral forces are available, and the path of the vehicle is thereafter handled by the longitudinal forces via providing a sufficiently large turn out moment during the maneuver.

Figure (3.15) shows that the vehicle in quasi-steady state braking follows the actual curvature, thus does not induce a rotation of the vehicle to build up lateral forces. Thus, sufficient lateral forces are already existing due to quasi-steady state braking.

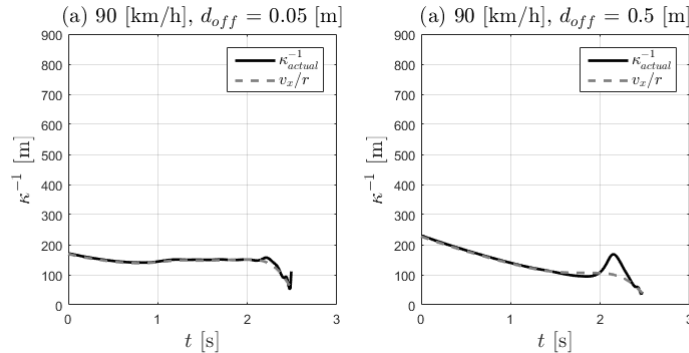


Figure 3.15:  $|\kappa^{-1}|$  compared to the effective radius for Optimal Controlled braking (OCB) for (a) an allowed off-tracking of 0.05 m and (b) 0.5 m for an initial velocity of 90 km/h and a corner radius of 150 m.

The quasi-steady state solution uses free initial boundary conditions and is therefore showing that the optimal way of braking the vehicle is performed when a sufficient magnitude of turn in moment and yaw rate, which confirms the transient behavior discussed in Section (3.4). One can observe a near linear decrease in longitudinal velocity over time history for the case of 90 km/h in Figure (3.14). This is due to that the longitudinal acceleration is high during the entire maneuver, since this case is far from the theoretical limit of cornering velocity defined in Expression (3.1). The magnitude of the longitudinal deceleration is therefore high during the maneuver, starting at  $0.9g$  for the case of  $v_0 = \sqrt{v_x^2 + v_y^2} = 90$  km/h. One can also observe that the peak value of yaw rate has been reduced compared to case of step braking seen in Figure (3.8) explained by less wanted rotation of the vehicle initially in the maneuver. The negative yaw moment from the longitudinal forces, discussed above, can be further observed in Figure (3.16) showing the time history for the braking force and the normalized force for the quasi-steady solution during the maneuver.

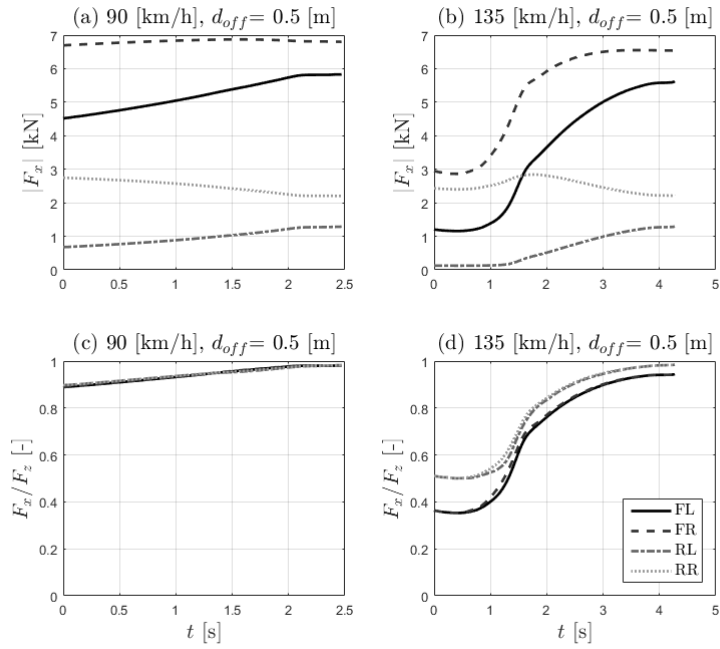


Figure 3.16: (a & b) shows braking forces for two cases. (c & d) are the normalized braking forces for the same cases. OCB was used with quasi-steady state initial condition.

In accordance with what have been stated previously it can be seen that a turn out moment is beneficial for obtaining the optimal brake solution for the braking in a corner scenario. It can also be seen that the transient behavior seen initially when applying the brake forces as a step is reduced and the brake forces are smooth over the time history; similar to how a real brake intervention is applied. The quasi-steady state solution showed similar results with the second phase in the step braking case. The force utilization difference between the front and the rear axle shows that more of the available grip shall be used on the rear axle compared to the front axle at higher speeds. This could be due to that at higher speeds there is a need to make the vehicle less understeered to complete the maneuver in an optimal way. By increasing the longitudinal forces on the rear axle, the turn out moment from the longitudinal forces increases while the turn out moment from the rear lateral forces decreases. The net result is however that the total turn out moment generated by the rear axle is decreased. This means that it is possible to generate more longitudinal deceleration while the turn out moment remains unchanged. The time history for the angle of the force vector acting on the vehicle during the scenario is visualized in Figure (3.17).

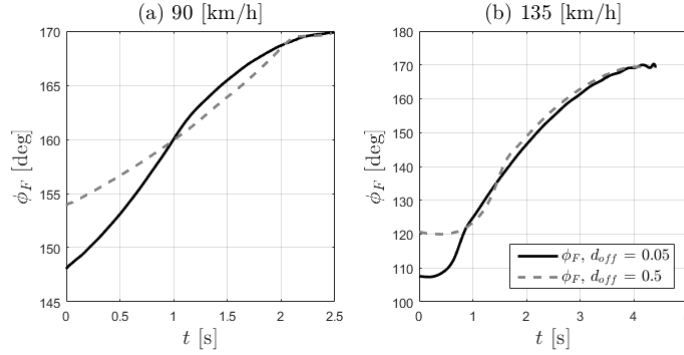


Figure 3.17: *Time history of the global force vector angle during the case of an initial speed of (a) 90 km/h and (b) 135 km/h for an allowed off-tracking of 0.5 m while driving in a curve radius of 150 m.*

From the analysis of the force vector angle it can be determined that a pronounced decrease of transient behavior in the lower velocity case occur. It can be seen that the vehicle can allocate more of the vertical load for longitudinal braking when a large off-tracking is allowed, seen as the increased initial value of the force vector angle. A small decrease in the force vector angle during the first part of the maneuver for the high velocity case is the behavior of how it handles the off-tracking. What can be seen is that it approaches the off-tracking limit at the beginning of the maneuver. After this phase it follows the off-tracking limit until stand still. When comparing the different off-tracking limits, it can be observed that a larger off-tracking limit yields a higher magnitude of longitudinal braking in the beginning of the maneuver. The force vector angle approaches  $170^\circ$  in the end of the maneuver, which was accepted since the side slip angle had an allowed magnitude of  $10^\circ$  and a force vector angle is therefore applied in the opposite direction for the total velocity vector. The force vector angle shows that longitudinal braking is prioritized towards the end of the maneuver, which is natural since the demand of lateral capability decreases with longitudinal speed, simplified as  $a_y = v_x^2/R$ .

A study of the sensitivity for quasi-steady solution was done in with respect to allowing a variation of side slip and road friction coefficients, which can be found in Appendix (C). The sensitivity analysis shows that the overall strategy for optimal braking in a corner has low dependency of the total road adhesion level. A decrease in braking distance can be achieved by achieving a larger slip angle during the maneuver. However, a vehicle cannot be controlled in a fashion where a large slip angle is desired. Due to the fact that similar trends were observed between the different imposed side slip constraints, it was concluded that a controller that is operating with low slip angles during the maneuver should be used in future applications.

### 3.6 Optimal Control Results Show Trade-off in Braking Distance versus Off-tracking

With the optimal solutions for individual wheels it was of interest to investigate how the results are affected by varying the allowed off-tracking. By investigating this, it was possible to evaluate the limitations of the scenario, to motivate the implementation of a sophisticated integrated brake controller utilizing an allowed off-tracking for decreasing the braking distance.

#### 3.6.1 Decreased Braking Distance by Introducing an Allowed Off-Tracking

The quasi-steady state solution for OCB solution was performed with a side slip constraint of  $\beta_{lim} = 10^\circ$ , which gave proper results regarding the behavior of the longitudinal force and the global force vector angle during the scenario. The deviation from the reference path with a certain allowed off-tracking yields a trade-off between braking distance  $d_b$  and the allowed off-tracking  $d_{off}$ . Depicted in Figure (3.18) is the Pareto fronts for three different initial velocities and a reference path with a curve radius of 150 m. Along the lines are the optimal solutions, points below the lines are not possible to reach and all points above these lines are sub-optimal [21]. The trade-off regarding braking distance and off-tracking stresses the differences between optimal braking solutions with the assumption of uniform road adhesion on all parts along the vehicle trajectory.

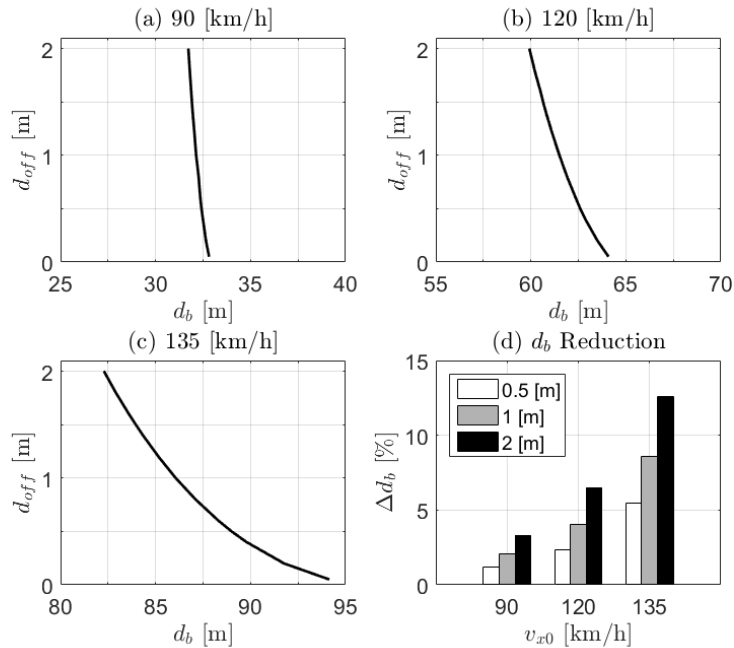


Figure 3.18: (a,b & c) Shows Pareto fronts of the trade-off between braking distance,  $d_b$ , and off-tracking,  $d_{off}$ , for three different initial velocities with a curve radius of 150 m. (d) Shows the braking distance reduction in percentage by allowing a certain off-tracking for the two track model.

The results show that the positive effects of allowing more off-tracking are more pronounced at higher initial velocities. The gain in braking distance for the case defined by an initial velocity of 90 km/h for an allowed off-tracking of 0.5 m, compared to the most strict off-tracking case of 0.05 m, was determined to be 1.2 - 3.3% by allowing an deviation between 0.5 - 2 m from the reference path, seen in the bar chart in Figure (3.18d). The percentage numbers corresponds to an decrease in braking distance of 0.40 - 1.07 m, seen in Figure (3.18a). Figure (3.18c) visualizes the gain for the cases with an initial velocity of 135 km/h and shows a large gain when comparing the most strict off-tracking case with an allowed off-tracking between 0.5 - 2 m. It is determined

that the braking distance can be decreased with 5.4 - 12.6%, corresponding to a gain of 5.14 - 11.90 m i actual braking distance decrease.

By allowing the vehicle to off-track, the velocity during the scenario can be decreased. Figure (3.19) shows the velocity history compared to the traveled distance and the velocity history compared to the most strict off-tracking case 0.05 m for travelled distance.

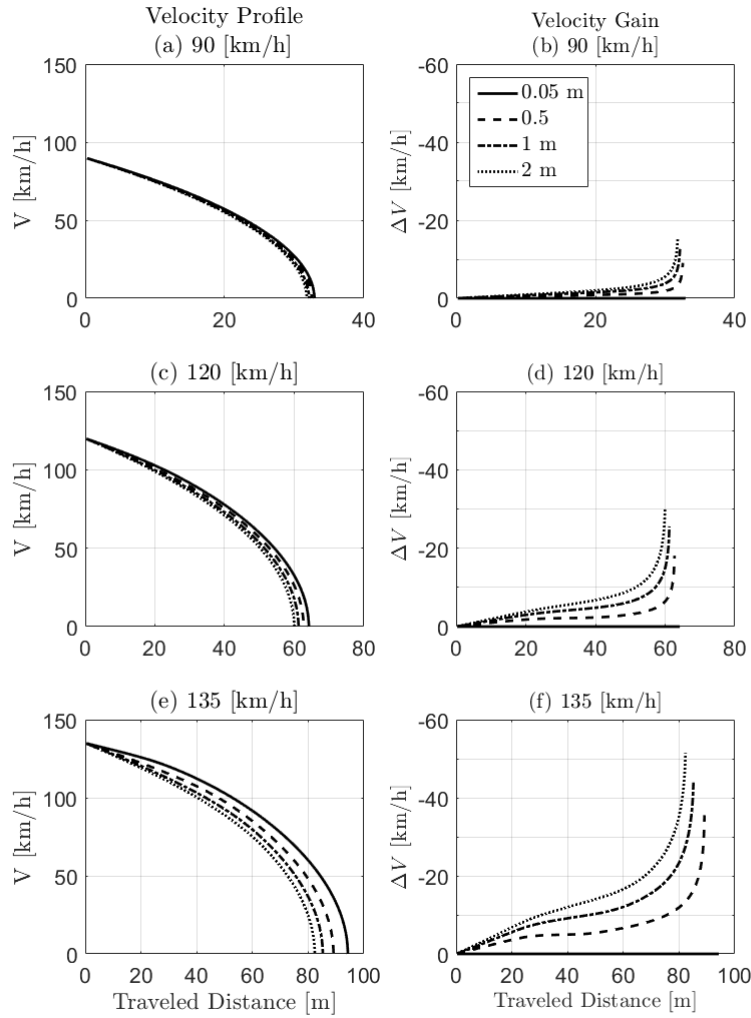


Figure 3.19: (a,c & e) shows velocity profiles for an initial velocity of 90, 120 and 135 km/h respectively, during the optimal brake intervention compared to travelled distance.(b,d & f) visualizes the possible decrease in velocity for an initial speed of 90, 120 and 135 km/h respectively, the during the brake intervention with respect to travelled distance compared to the most strict path following constraint of 0.05 m.

From the figure it can be concluded that an allowed off-tracking decreases the velocity during the intervention. Figure (3.19) yields that a possible safety benefit can be obtained if the vehicle is braked optimally for an allowed off-tracking of 0.5 - 2 m. From Figure (3.19(b)) it is concluded that a vehicle that allows 1 m off-tracking has a  $\Delta V = -10$  km/h after  $\sim 32$  m of travelled distance. Further explained as; if an object is positioned at 32 m from the host vehicle at the start of the brake intervention the impact velocity is decreased by 10 km/h comparing the most strict path following constraint and the 1 m allowed off-tracking case. The possible velocity gains increases with speed and off-tracking and the highest velocity gain is determined to  $\Delta V = -51$  km/h after  $\sim 82$  m for the case of an initial speed of 135 and allowed off-tracking of 2 m. An allowed off-tracking yields a decreased velocity during the brake intervention, and therefore also a decreased stopping time. The reduction for stopping time for the two track model with imposed side slip constraint is seen in Figure (3.20)

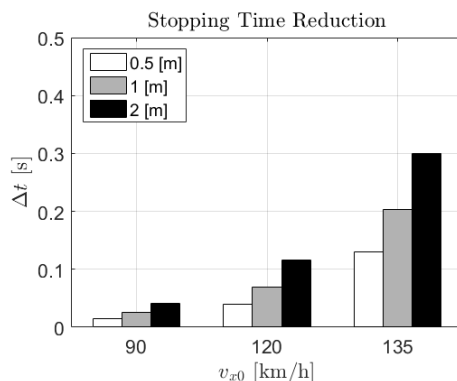


Figure 3.20: *The optimal solution when allowing a certain off-tracking gives a stopping time reduction.*

A small reduction of stopping time can be established if the vehicle is allowed to off-track from the reference path. The reduction in stopping time was concluded to be increasing with speed with the smallest gain of 0.014 s when off-tracking 0.5 m from the initial speed of 90 km/h up to 0.30 s time reduction for off-tracking 2 m in 135 km/h. To put this reduction of stopping into a context; real world studies has shown that the drivers limit of trying to perform a collision avoidance maneuver is 1 down to 0.8 s and that an possible braking intervention should be applied when exceeding the lower limit [22].

### 3.6.2 Transient Phase Shows Larger Gains in Braking Distance, Velocity Decrease and Stopping Time

Aside from the quasi steady results, a comparison was also made of the optimal results including the transient phase. When including this phase the possible gains by off-tracking were larger. In Figure (3.21) it can be observed that there is a slight increase in braking distance at smaller off-tracking values than compared to the quasi-steady state Pareto fronts in Figure (3.18). This is due to that when initiating the scenario from steady state cornering, the case of a smaller allowed off-tracking needs a larger yaw rate to follow the path which means that it has to create a larger yaw moment which in turn reduces the deceleration possibility. This difference between the cases is smaller when the scenario starts at quasi static state since the initial boundary on yaw rate is free resulting in that different cases has different initial yaw rates, thus removing the large yaw moment differences at the beginning of the maneuver. This results in a lower deceleration initially in the maneuver when the initial conditions are set as steady state cornering and this is what yields the longer braking distances.

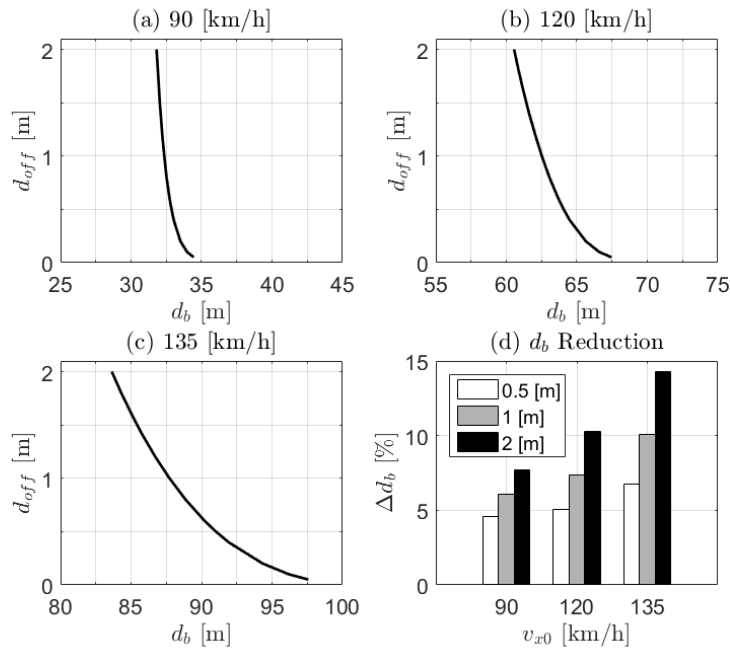


Figure 3.21: Trade-off curves from simulations with transient behavior initially. (a, b & c) Shows Pareto fronts of the trade-off between braking distance,  $d_b$ , and off-tracking,  $d_{off}$ , for three different initial velocities with a curve radius of 150 m. (d) Shows the braking distance reduction in percentage by allowing a certain off-tracking for the two track model.

The build up of a positive yaw rate in the beginning of the maneuver for starting for steady state cornering gives less longitudinal force for decelerating the vehicle as discussed earlier. The velocity gain is also affected by the initial build up of a certain yaw rate. For the case of initial conditions based on constant steady state is giving a velocity gain of 20 km/h after 32 m into the scenario for and off-tracking of 1 m compared to the most strict path following constraint with an initial speed of 90 km/h in a corner of 150 m. The stopping time is therefore also reduced for off-tracking for the step braking from steady state cornering, giving a possible reduction of 0.06 - 0.1 s for an allowed off-tracking of 0.5 - 2 m compared to the most strict following path constraint for the initial speed of 90 km/h with a corner radius of 150 m.

## 4 Control Design

The trade-off analysis regarding braking distance versus off-tracking showed that a gain in braking distance, stopping time and velocity decrease can be achieved by allowing a certain off-tracking. This motivates an investigation of brake controller utilizing the allowed off-tracking for reducing the braking distance.

A general integrated motion control covering more scenarios could be based on control allocation. Control allocation is explained as an optimization of actuator coordination for an over actuated system, i.e. the number of actuators is larger than the degrees of freedom [23]. Control allocation has historically been used in aerospace and marine engineering but has also been used in research regarding the automotive vehicles [24][25]. The control allocation optimizes the coordination of the actuators in order to meet the demands from the driver or other control intentions. The control allocation can therefore divide the control task in modules in order to meet the required motion from a higher level control system. Previous research of minimizing the maximum off-tracking when overspeeding into a corner has shown that the global force vector angle shall be kept constant during the scenario [17]. Research of utilizing this force vector angle in a continuous controller for a avoidance maneuvers, via control allocation for the individual wheel forces, has shown promising results [26]. The controller proposed below is a simple interpretation of such a force vector angle controller and could be converted into a control allocation controller.

### 4.1 Optimal Control with Particle Representation

This section explains a derived particle representation and the optimal control results using the particle representation for the scenario of deceleration while cornering. By the use of a particle representation one neglects the transient behaviour seen in the results from vehicle model, since a particle representation does not have yaw dynamics. Using a particle reference for a controller could therefore reduce the transient behaviour. Hence, only utilize the quasi-steady braking where the accelerations changes slowly. This approach for the design of a controller is therefore more likely to be used in a real vehicle. The equations of motion for the particle can be seen in Expression (4.1). It was derived with two external forces acting on the particle. The particle has no yaw dynamics and was constrained to utilize the road adhesion fully. The parametrization of the particle representation is found in Figure (4.1) where the angle  $\phi_F$  was used as the control variable, i.e. directing the acceleration in the inertial reference frame.

$$\begin{aligned} F_x &= -ma_x \\ F_y &= ma_y \\ (\mu g)^2 &= a_x^2 + a_y^2 \end{aligned} \tag{4.1}$$

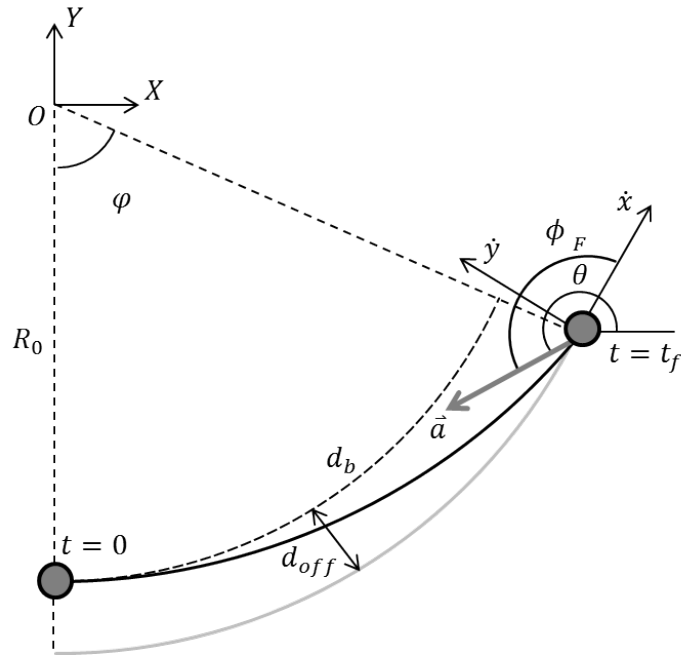


Figure 4.1: *Parametrization of the particle representation of the optimal control problem*

The optimal control solution for the particle representation of the problem at hand is named Optimal Control Particle, abbreviated OCP. The optimal control maneuver for the two track (OCB) and the particle model (OCP) was compared for the case;  $V_0 = 90$ ,  $R_0 = 150$  m with an allowed off-tracking of 0.5 m. The trajectory and the lane utilization, in the inertial reference frame, is shown in Figure (4.2).

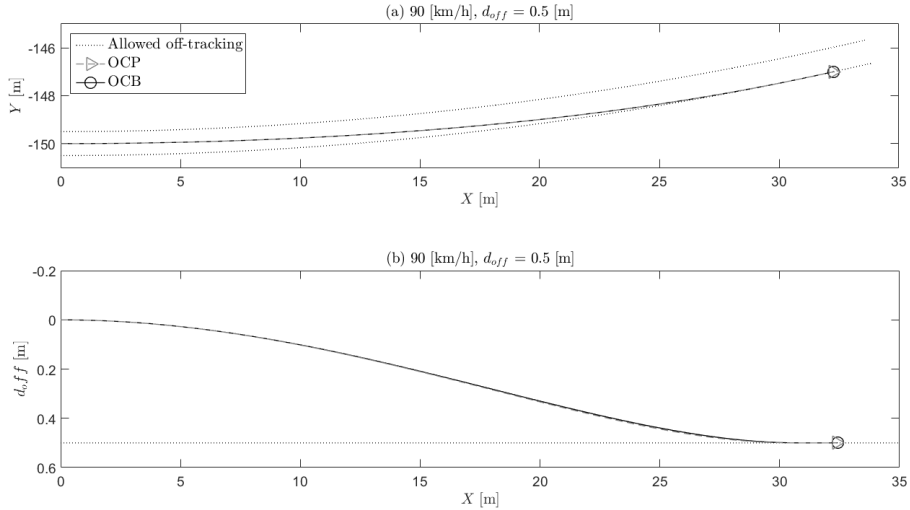


Figure 4.2: *Trajectories and lane utilization of the case of 90 km/h, 150 m radius and an allowed off-tracking of 0.5 m for the particle (OCP) and two track model (OCB).*

From the trajectories and the lane utilization over the travelled distance it can be found that optimal particle solution coincides with the optimal braking solution for the particle for the chosen case. The similarities regarding optimal path of the particle and two track results are consistent over the entire speed range up to a

velocity near the velocity limit,  $v_{lim}$ . The similarities in optimal path solution motivates the use of a particle model to derive the possible paths in future vehicle applications. The braking distance for the lower speed case of 90 km/h and the high speed case of 135 km/h for the particle representation was concluded to be 32.38 m and 88.75 m respectively and for the two track 32.42 m and 89.00 m, where the ideal braking distance was calculated from conservation energy, seen in Appendix (B), to 31.9 m for the case of 90 km/h and 71.7 for the case of 135 km/h. Another comparison has been done observing the time history of force vector angle can be seen in Figure (4.3).

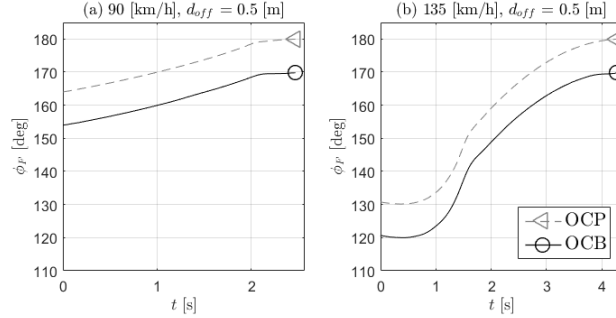


Figure 4.3: Force vector angle for the OCP and OCB for a curve radius of 150 m in a initial velocity of (a) 90 km/h and (b) 135 km/h.

The force vector angle derived from OCP and OCB has an offset equal to the side slip constraint used for the two track, which was set to  $\beta_{lim} = 10^\circ$ . The use of a less time consuming path and braking solution through a particle representation is therefore promising, given that a quick buildup of lateral force is provided to make use of the vertical force for longitudinal deceleration early in the maneuver.

Figure (4.4) shows the velocity profile for the time history of the maneuver in the case of 90 km/h and 135 km/h with an allowed off-tracking of 0.5 m with  $R_0 = 150$  m.

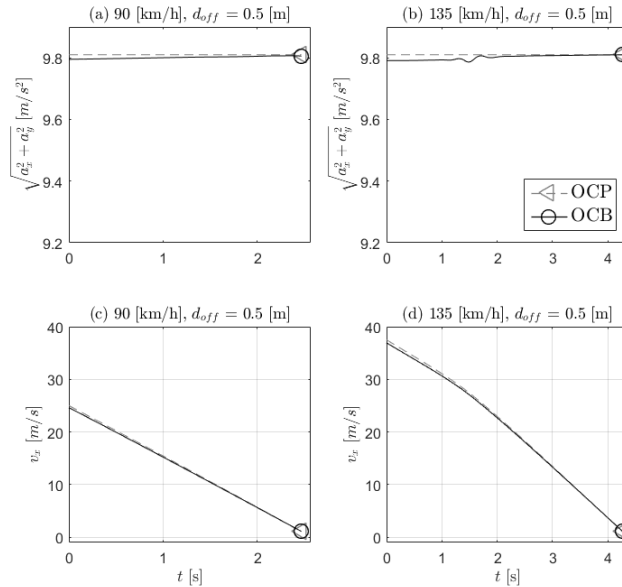


Figure 4.4: (a & b) total acceleration magnitude and (c & d) velocity profile for the particle representation and two track model for two cases with initial speed of 90 km/h and 135 km/h respectively.

The acceleration magnitude for the two track model is lower than the particle representation, which utilizes the

road adhesion fully, due to the yaw dynamics of the two track model. However, a high level of road adhesion can be observed due to the large lateral forces from  $t = 0$  s. The velocity profiles are therefore almost identical and show a close to linear shape for the low velocity case and small bent shape for the higher velocity. A analytical derived velocity profile for the particle could serve as a reference in a future controller [17]. However, an expression for the velocity profile has not been derived. The particle representation and the two track model has shown almost identical solutions over the whole range of velocities which adds a confirmation of that a true optimality solution has been found, and therefore can be useful in future control of the vehicle motion.

As described earlier; the particle representation always utilizes full road adhesion. This yields a starting point for a brake controller for the two track model. The optimal solution of strict path following, for a particle representation, is captured by observing the lateral acceleration, available friction and the amount of vertical load. The allocation of the total road adhesion in longitudinal and lateral forces must be done in accordance with the wanted lateral acceleration defined by the curve radius and the velocity. The total amount of road adhesion is defined by the road surface friction seen in Expression (4.2), where  $f_b$  corresponds to the longitudinal allocation factor, which is the normalized longitudinal acceleration.

$$\begin{aligned} f_b &= \sqrt{1 - \left(\frac{a_y}{\mu g}\right)^2} \\ a_x &= f_b \cdot \mu g \\ a_y &= \sqrt{1 - f_b^2} \cdot \mu g \end{aligned} \tag{4.2}$$

With the  $a_y$  representing the wanted lateral acceleration from interpreting the drivers steering wheel input or given from a path reference. The trivial case of strict path following while assuming full road adhesion, as for the particle, is therefore prioritizing lateral capability early in the maneuver where after the longitudinal velocity decreases, more is allocated to longitudinal braking, which is a direct correlation to the friction circle. The longitudinal allocation coefficient and the global acceleration vector angle,  $\phi_F$ , is visualized in Figure (4.5) for the objective of minimizing longitudinal speed, constrained to follow the path.

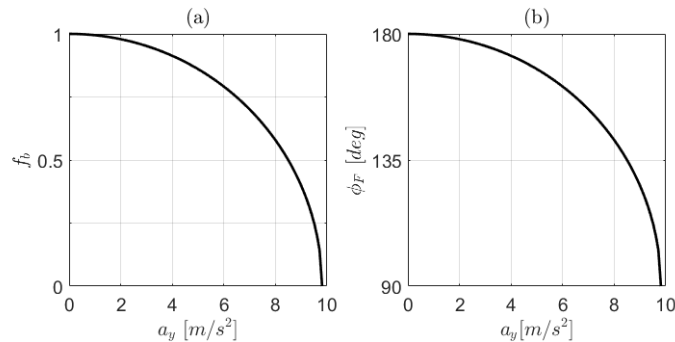


Figure 4.5: (a) The ideal allocation of longitudinal utilization of the road adhesion for trivial case full road adhesion utilization of path following. (b) global force vector angle during the a brake intervention with an objective of minimizing longitudinal speed and follow the intended path strictly

The use of a force vector angle, or a longitudinal allocation factor can be realized via control allocation [26].

## 4.2 Particle Representation Yields Strategy for Control

The optimal control results for the particle representation, regarding the level of longitudinal acceleration during the maneuver, showed similarities with the vehicle model. As observed in Figure (4.3) the force vector angle was similar but with an offset because of the imposed side slip constraint on the vehicle. When the

particle reaches the off-tracking limit, the allocation factor,  $f_b$ , has a distinct look and it increases when the velocity decreases. A further analysis was however needed to understand how the allowed off-tracking affects the force angle at the beginning of the maneuver, when it has not yet reached the off-tracking limit.

The path curvature  $\kappa$  of the trajectory taken by the particle was calculated according to the Expression (4.3). The Expression (4.4) was then used to calculate the demanded lateral acceleration for following the curvature.

$$\kappa = \frac{|v_x a_y - v_y a_x|}{(v_x^2 + v_y^2)^{3/2}} \quad (4.3)$$

$$a_y = v_x^2 \kappa \quad (4.4)$$

In Figure (4.6) it can be observed that the particle follows the friction circle during the whole maneuver.

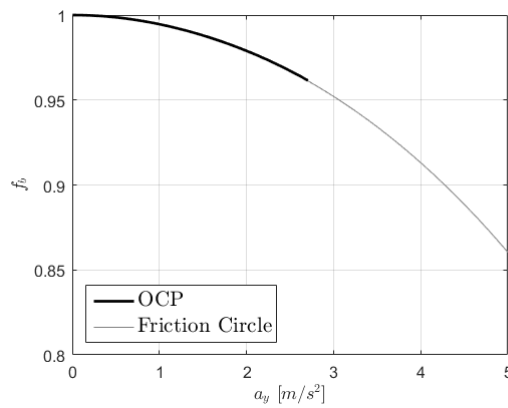


Figure 4.6: Allocation factor for optimal control of particle in the case with an initial speed of 90 km/h and an allowed off-tracking of 0.5 m

This concludes that to obtain the optimal path reference, it is a strictly geometrical problem based on the initial conditions and the allowed off-tracking. Therefore, the controller is based on the friction circle allocation and a wanted radius determined by the allowed off-tracking.

Using the earlier Expression (4.2) one can define a wanted longitudinal braking factor based on the needed lateral acceleration to stay on the intended path. This will generate a deceleration profile based on the wanted path and the curvature of that path. A simple brake controller was designed to emulate full use of the road adhesion during the whole scenario, equivalent to the particle representation where all grip not used for lateral acceleration is demanded as longitudinal deceleration. The control input to the simple controller was the path radius from the particle representation from which it is possible to calculate the needed lateral acceleration. The wanted curve radius was taken from the optimal control results from the particle representation i.e. using the particle as the reference model for the scenario, according to Expression (4.5). The expression shows the function  $f$  which correlates the angle  $\varphi$  defined in Figure (4.1) to the wanted radius  $R_w$ .  $\varphi$  represents the angle along the reference circle that the vehicle has travelled and was used as the control to mimic the off-tracking behaviour seen in the particle representation.

$$R_w = f(\varphi) \quad (4.5)$$

$R_w$  is defined as the wanted curve radius and is used in Expression (4.6) to calculate the desired longitudinal deceleration. This longitudinal allocation factor is based on the wanted radius  $R_w$  during the maneuver, where lateral acceleration is described as  $v_x^2/R_w$  assuming quasi-steady state conditions. The longitudinal allocation

factor is seen in Expression (4.6), derived from Expression (4.2).

$$f_b = \sqrt{1 - \frac{v_x^4}{(\mu g R_w)^2}} \quad (4.6)$$

This approach is always trying to combine all available road adhesion to either longitudinal or lateral acceleration. The friction coefficient  $\mu$  must therefore be determined for a successful controller implementation. The calculation of a force vector angle from the longitudinal allocation, for implementation in a more sophisticated controller, can be seen as the motivation behind the longitudinal allocation factor approach.

#### 4.2.1 Open Loop Implementation of the Acceleration Magnitude Reference

The implementation of the the longitudinal allocation factor as a controller was named Acceleration Magnitude Reference, abbreviated AMR. The implementation of the AMR controller in a vehicle is out of scope of the thesis; however a suggested simplified implementation of the feed-forward controller for the longitudinal braking factor is proposed here. A proportional gain on each tire was tuned with a genetic algorithm with the main objective of minimizing the braking distance and minimizing the off-tracking limit. The gains on each wheel is used in order to handle the wanted yaw moment and yaw rate during the maneuver, seen to have a major role in minimizing the longitudinal deceleration.

The open loop AMR controller was based of wanted radius, for following an expected longitudinal acceleration profile, previously described. The longitudinal force on each wheel used in the open loop solution is displayed in Expression (4.7).

$$F_{xij} = -\gamma_{ij} \cdot f_b \cdot \mu \cdot F_{zij} \quad i = 1, 2 \text{ and } j = l, r \quad (4.7)$$

From Figure (3.16), showing the longitudinal forces, it can be observed that there is a proportional gain difference between the forces. The differences was handled by the  $\gamma$  factors, determined by the genetic algorithm. The proportional gains for the case of 90 km/h with an allowed off-tracking of 0.5 m was determined:  $\gamma_{1l} = 0.918$ ,  $\gamma_{1r} = 0.975$   $\gamma_{2l} = 0.869$  and  $\gamma_{2r} = 0.998$ . The proportional gains for the case of 135 km/h with an allowed off-tracking of 0.5 m was determined:  $\gamma_{1l} = 0.993$ ,  $\gamma_{1r} = 0.761$   $\gamma_{2l} = 1.00$  and  $\gamma_{2r} = 0.611$ .

## 5 Control Performance Evaluation

To evaluate the proposed controller (AMR) a comparison between it, the optimal control solution for a two track model (OCB) and the reference system (FBPS) was done. The controller was compared to the optimal control solution results shown in Section (3.5) and to the reference braking system described in Section (3.2).

The proposed AMR controller shows a good correlation to the optimal control results in terms of braking distance for the case of 90 km/h with an allowed off-tracking of 0.5 m, starting from quasi-steady state conditions. The side slip during the maneuver with the AMR controller showed  $\max(|\beta(t)|) \leq 5.8^\circ$  during the maneuver with an initial velocity of 90 and 135 km/h. It was therefore decided to compare the AMR controller with the OCB solution with an imposed side slip constraint of  $\beta_{lim} = 5^\circ$ . The comparison between AMR and OCB shows less visible similarities in the case of 135 km/h, where the AMR controller showed a maximum off-tracking of  $\sim 1.5$  m. Figure (5.1) displays the trajectories for the different strategies. When controlling the steer angle optimally with a fixed brake proportion (FBPS) the result shows that the desired path can be maintained with respect to allowed off-tracking but the braking distance is larger than both OCB and AMR. A large braking distance for the reference system is due to the maintained lateral capability of the select low feature. However, this situation depicts the optimal way of controlling the steering wheel and brake pedal which means this is a very difficult maneuver for a driver to execute due to large and quick steering maneuvers. The braking distances for these cases are also shown in Table (5.1).

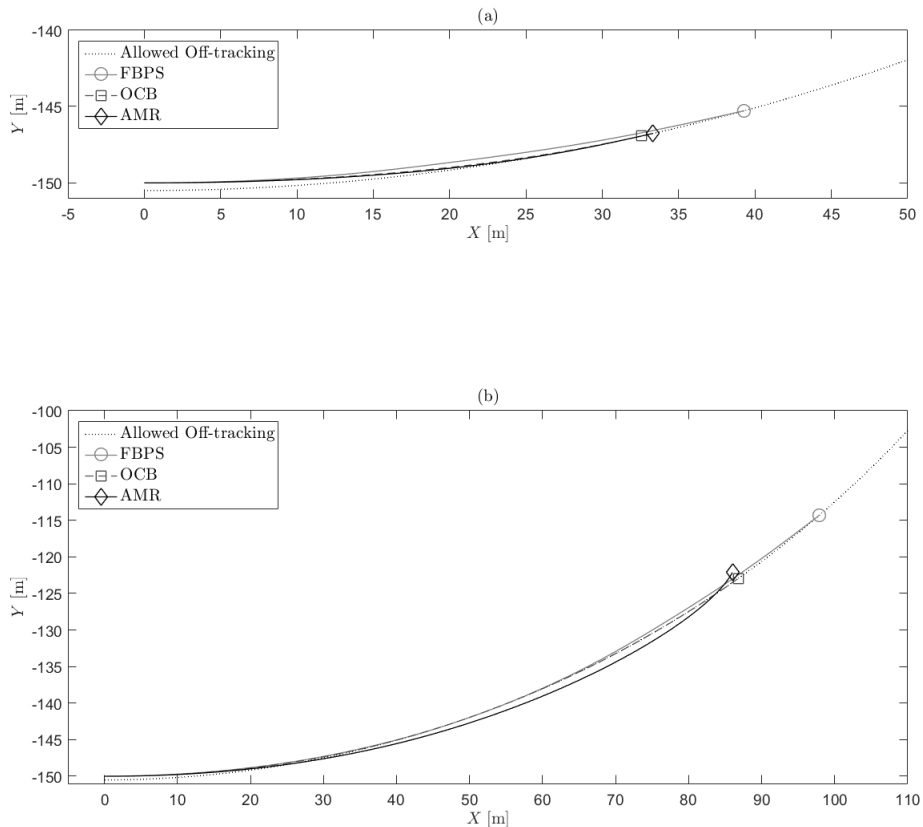


Figure 5.1: Trajectories for (a) 90 km/h and (b) 135 km/h.

Table 5.1: *Braking distances for two cases with an allowed off-tracking of 0.5 m*

$d_{off} = 0.5 \text{ m}$	FBPS	OCB	AMR
90 km/h	39.6 m	32.7 m	33.5 m
135 km/h	106.3 m	92.2 m	92.0 m

Almost all strategies were able to handle the scenario of keeping the maximum off-tracking to 0.5 m in an initial velocity of 90 km/h. The AMR controller is however deviating from the allowed off-tracking with  $\sim 0.012 \text{ m}$  but shows fairly good correlation to the optimal results in terms of lane utilization seen in Figure (5.2). For the case of 135 km/h, only the OCB and FBPS was able to maintain the allowed off-tracking. The AMR controller could not mimic the behavior of the optimal results. Observing the lane utilization as depicted in Figure (5.2b) it can be seen that the AMR controller does not coincide very well with the optimal control results at 135 km/h. The look of the lane utilization for the AMR controller in this case can be explained by the use of fixed gains on each wheel. These gains where most gains have a value below 1. Thus, braking force on each wheel can therefore not reach full maximum braking which increase the braking distance and gives a too large lateral capability at the end of the maneuver, seen as a small turn in at the end of the maneuver, most noticeable in the 135 km/h case. This is not a desired motion, since the most of the vertical force could be allocated to the longitudinal deceleration at the end of the maneuver. One can also conclude that the AMR controller was not able to produce a desired yaw moment and yaw rate initially, which leads to a too large off-tracking.

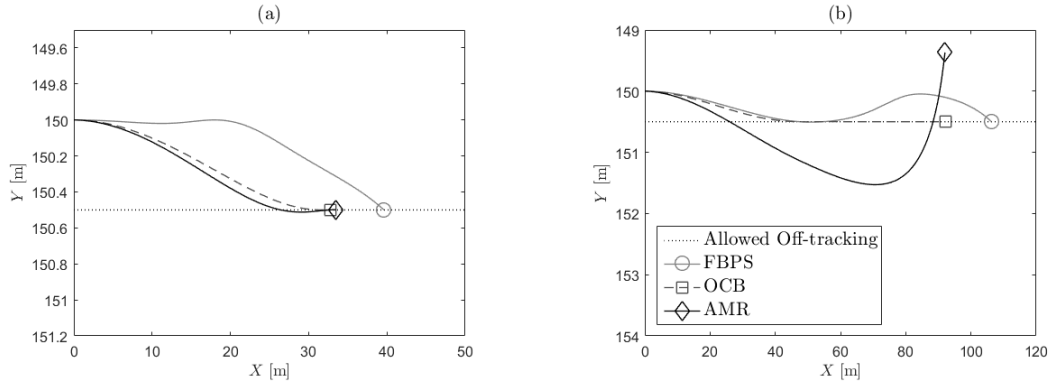


Figure 5.2: *Lane utilization for the OCB, AMR, FBP and FBPS in an initial velocity of (a) 90 km/h and (b) 135 km/h in a corner radius of 150 m.*

The FBPS reference travels towards the outside of the lane late in the manoeuvre, it is even turning into the corner more in the beginning which points at that the optimal driver would try to straighten the vehicle path to minimize the effects of a select low system due to lateral load transfer. By observing the normalized force on each tire, one can see that the AMR reference and the optimal control shows similar behaviors in the lower speed case but a difference can be observed as the initial speed was increased.

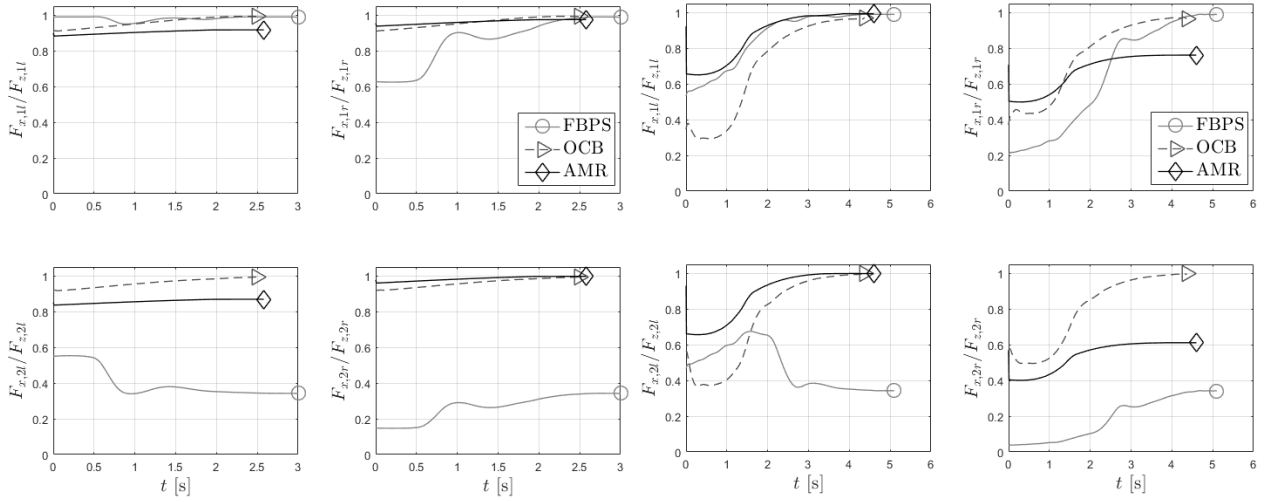


Figure 5.3: Longitudinal force utilization for the case of 90 km/h seen as the four figures to the left. Longitudinal force utilization for the case of 135 km/h seen as the four figures to the right.

The fixed gains on each wheels generated with a genetic algorithm yields gains that makes sure that the overall look of the curve is close to the optimal. Variable gains on each tire could therefore help to adjust the curve to coincide over the whole time history. Figure (5.4) shows a comparison of the force angle history for the different systems.

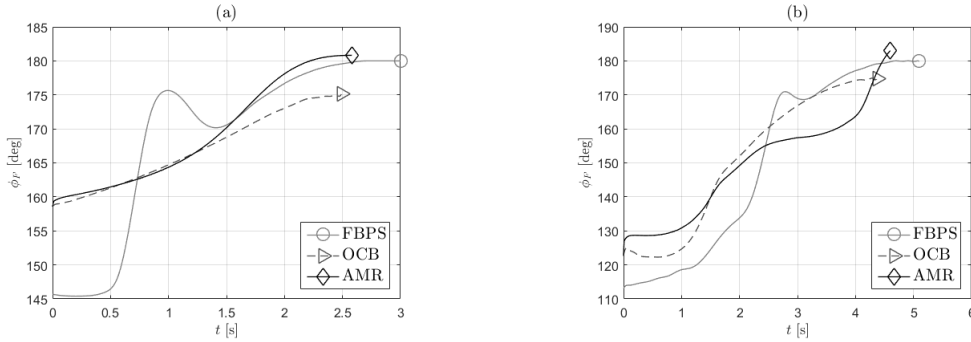


Figure 5.4: Force vector angle comparison for the OCB, AMR, FBPS and FBPS in a initial velocity of (a) 90 km/h and (b) 135 km/h.

It can be observed that the reference case uses a lot of lateral grip in the beginning of the manoeuvre, but after this initial phase uses more longitudinal grip. This coincides with the results of lane utilization where the reference stays in the middle of the lane for longer. This could be a result of the select low strategy, leaving more grip for lateral capability which can also be observed in Figure (5.3).

The difference between the optimal result and the AMR controller in force vector angle is due to that the optimal results has larger side slip values at the end of the manoeuvre which was not obtained with the AMR controller. A reason for that the AMR controller does not coincide very well with the behaviour of the optimal control results could be the radius used as the set point. In Section (4.2) it was concluded that the important parameter to use from the particle representation is a good path reference, which was the reason for using the particle path as feedforward for the controller. Better results may be achieved if the allocation factor itself would have been used as feedforward input to the controller. However, as explained by Figure (4.6) the optimal control solution for particle representation has shown to be close to a strict geometrical problem. The comparison for the vehicle states between the optimal solution and the AMR controller is visualized in Figure (5.5).

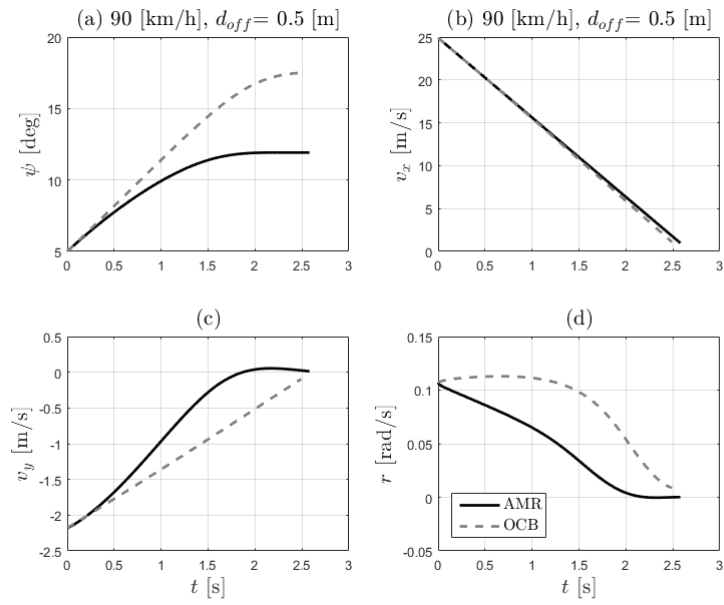


Figure 5.5: *Time histories of selected states for the optimal control results (OCB) and the AMR controller in the case of 90 km/h.*

The comparison results for the vehicle states shows poor similarity between the AMR controller and the optimal solution, which points at that a better feedforward variable could be used. A more sufficient representation of the wanted radius, that is updated continuously, would give a better initial yaw moment build up for mimicking the optimal solution.

## 6 Discussion

The optimal brake control results shows that a turn out moment from the longitudinal braking force appears as a consequence due to maximizing deceleration. The results showed that the wheels on each axle should use approximately the same proportion of the vertical load to decelerate the vehicle. Because of the load transfer that the vehicle is experiencing, this results in a higher brake force on the outer wheels compared to the inner wheels. Thus, a turn out moment is created. To counteract this there is a need of an initial buildup of a turn in moment and a large initial yaw rate to be able allocate as much of the vertical force as possible for longitudinal usage during the rest of the maneuver. This result means that, to perform this maneuver optimally, there is a delicate balance between a buildup of yaw moment and yaw rate from the lateral forces and a turn out moment from the longitudinal forces.

In the initial optimizations that were done, a transient phase was observed. The transient occurred due to the need of yaw rate and turn in moment early in the maneuver. A future controller implementation will not be designed with a transient as a set point. A controller would instead have a smoother transient, either a ramping function or that the algorithm is activated after the driver has already initiated the braking intervention. The transient phase was therefore neglected in later optimizations by removing some of the initial boundary conditions in the model. This means that the simulations did not start from steady state cornering conditions but from quasi-steady state braking conditions, which is the assumption that the braking intervention has already been ramped up and that the transient phase is neglected. This means that the differences between how the strategies reaches the quasi-steady state were neglected and could affect the results since the wanted initial lateral force and yaw rate buildup was assumed to be present from  $t = 0$  s. Instead of using these free boundary conditions to obtain a non-transient phase, it could be possible to impose a constraint on yaw acceleration or yaw moment to achieve a non-transient phase.

The transient behavior could also be questioned by the fact that the vehicle model is quasi-static. In a more detailed vehicle model, with suspension effects with damping, this phase would probably have another look. The simplicity of the model could also be a cause for concern in terms of the validity of the results. Since the tire model is a simple degressive model there is no distinct peak in lateral grip, which is a reason for the high side slip levels discussed in Section (3.4). A reason for the use of such a simple model is to establish the general trends and motions involved in the scenario. If these are not visible or traceable for a simple model there is no use in pursuing the same trends with a more advanced model. Using a simpler model which is better behaved, in the sense of continuous and differentiable equations, helps or is even required for the convergence of the optimal control solutions. A more advanced vehicle model might reduce the need of constraints in the optimization, but is however adding complexity at the same time.

In the simple controller proposed, the wanted radius that the acceleration profile is generated from the particle representation off-line, as a lookup table. This is a very simple implementation. However, using the particle as a reference should be possible to do on-line in a vehicle as well. This could be done using a spiral equation starting from the initial radius and increasing to the set off-tracking at an arbitrary distance ahead to generate the desired path. This distance needs to be established from further analysis from the optimal control solution. The wanted radius or curvature for calculating the allocation factor should then be based on the curvature of the intended path. The wanted lateral acceleration could also be used to decide the brake distribution front/rear or just the distribution of brake forces. Taking the yaw moment into consideration would give better performance. Although the proposed, naive, controller shows varying results compared to the optimal solution, the particle representation shows potential of being used as a path reference in later applications.

The comparison to the reference system shows promising results. However, a better reference braking system, in terms of a variable brake distribution factor might be considered. Thus, EBD braking which ensures that no locking of the axles occurs would be a better representation of a state of the art system. Solving the optimal case of EBD braking with PROPT was made, without reaching convergence. A fixed brake proportioning factor was therefore established between front and rear, considered to utilize much road adhesion on the front axle. A large front shifted brake distribution was set due to the large magnitude of longitudinal acceleration from the start of the brake intervention for the case of 90 and 135 km/h in a corner radius of 150 m. The large magnitude of longitudinal acceleration gives instant load transfer due to the suppressed suspension effects.

When using the quasi-steady boundary conditions for the vehicle model, it can be seen that the results for OCP and OCB coincides very well. Even using the steady state initial conditions, giving transient behavior, shows

similarities but since the vehicle model has to handle yaw dynamics in the beginning of the maneuver which offsets the similarities. What can be learned from this is that at high levels of lateral capability, the vehicle model can be simplified as a particle representation. This notion could be used in autonomous function to evaluate path availability and possibly postpone the point of intervention. With cars having better performance from new and more powerful actuators e.g. electric motors and EPAS, the vehicle model and particle representation could show even more similarities. The computation time is also greatly reduced for a particle representation which can be used to increase the number of paths that is possible to evaluate.

If a control system similar the AMR controller, evaluated in this thesis, would come to market there is still a need for overall advanced controller logic to be able to handle different variations of this scenario. The investigation has showed that a gain in braking distance could be achieved through allowing a certain off-tracking from the reference path. However, if an obstacle would appear suddenly and all possible paths "closes" and the vehicle is able to understand that there will be an unavoidable crash, the motion priority might change and the priority in lane utilization might be thrown out the door and changed to a motion priority of minimizing the energy in the crash. Maybe it would even be beneficial to run off the road to avoid the crash, even if that sound unlikely. This type of controller would put high demand on the vehicles ability to predict road conditions ahead and to the side of the vehicle, since there is a risk of that the roadside could be dirty and that the available friction would be lower in more unused parts of the road width. A potential use of electric drive line for state estimation, such as the friction coefficient and wheel speed has shown to be useful. Mainly due to the accurate torque estimation that an electrified drive line provides. This leads to potential improvements in vehicle performance in the longitudinal and the lateral direction, compared to an conventional drive line [27].

Many advantages are seen with a common view of the vehicle state. An integrated control without many interfaces to other systems and control units could therefore provide car manufacturers with a possibility to less time consuming design iterations where the actuation and the decision of the wanted motion is separated, as in the function architecture example, seen in Figure (6.1). In this figure, the vehicle motion priority performed in the project, would therefore be positioned in the block named Vehicle Motion Priority.

If an integrated vehicle motion control unit provides the actuators with information, less tuning is needed between different interfaces and less dependency to *one* OEM can be established. An integrated control is seen as a step towards a safer, more costumer satisfying and potentially higher profit for the car manufacturer, where the control/ software can easily be changed without a need of extensive rearrangement of the vehicles function architecture and the actual actuators.

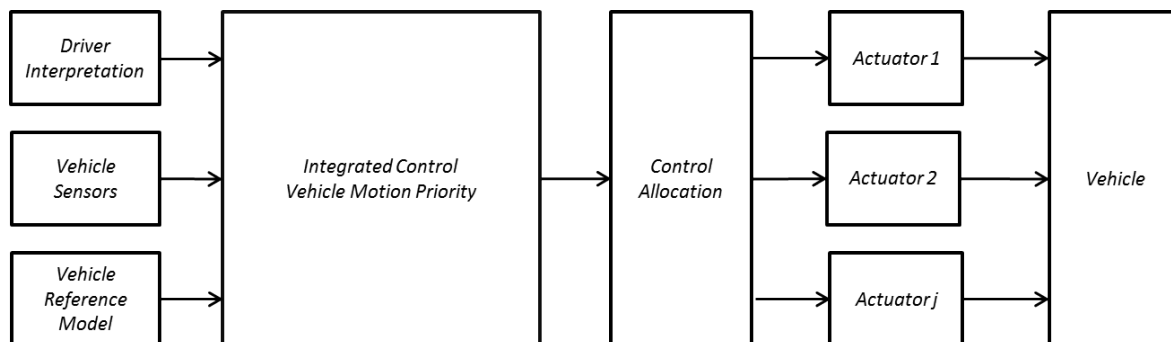


Figure 6.1: *Example architecture of a future implementation with integrated vehicle motion control, where the wanted vehicle motion is unanimously decided at a high level with knowledge about surroundings and driver intentions*

In the future, when drive-by-wire system are more accepted and developed, this type of integrated vehicle motion control will be possible by the use of control allocation. Research is being done on a general control allocation method for a vehicle that inputs a force vector angle and outputs four individual brake forces [26]. This research combined with the example function architecture seen in figure (6.1), can help in the removal of low level contradictions by the use of an high level decision making where the control allocation is only actuating the desired vehicle motion. As long as the driver and the high level situation interpretation can supply the low level control with one unanimous motion desire based on a high fidelity reference model, the contradictions at high level could be minimized as well.

Vehicle systems of today use signals from inertial measurement unit to maintain maneuverability and stability. In the future there might be a possibility of utilizing the force vector angle to follow the path based on intentions from the driver, infrastructure, etc. A system that monitors the allowed off-tracking and brakes accordingly may with advantage be used to provide a safety benefit. Such a system could therefore primarily be regulated using the global position and evaluating different paths, rather than using the inertial measurement systems. If a large variation of scenarios is going to be handled, it puts high demands on the control of the vehicle, but also the information provided to take decisions. The vehicle therefore requires information with a high confidence level together with an advanced control technique.

The velocity decrease, by allowing a certain off-tracking, may be seen as the major driving force behind introducing a braking system that make use of the allowed off-tracking, since a reduction of kinetic energy might change the outcome in a possible collision. If the front object is a vehicle standing still, a rear end collision is imminent. Neck injuries are most common in rear end collisions are the largest cause of disability of the occupants regarding a vehicle equipped with modern safety systems [28]. Whiplash injuries (WAD - Whiplash Associated Disorders)) are usually defined as AIS1 (Abbreviated Injury Scale, lowest level of injury). The whiplash symptoms differs in severity from short term stiffness in the neck to long term with severe neurological symptoms, but also reduced functions in reflexes, weak muscles that in the long run can cause mental illness [29]. Rear end collision was responsible for causing 800 000 neck injuries during 2010 in the EU27, where each case cost the society approximately € 3 719 [30]. A reduction in rear end collision could therefore decrease the number of neck injuries and also reduces the economic burden for the society. A "limit of harmfulness" in a two-vehicle rear impact has been concluded to a change of velocity during the impact between 10 - 15 km/h [31]. However, it is not possible to determine the severity of the collision based on only kinetic energy since the amplitude and shape of the acceleration pulse has shown to play a major role [32]. Therefore, no conclusions, regarding the safety benefit, can be made by only observing the velocity reduction. Another aspect of the velocity reduction by allowing a certain off-tracking can be seen as the differences in impact type. If the vehicle is off-tracking a possibility of a small overlap injury may appear, changing the characteristics of the impact which may worsen scenario. A trade off between impact velocity and the level of overlap will therefore need further investigation.

From the analysis of the velocity gain in the scenario, the potential gain is bigger in the end of the maneuver. The possibility of utilizing this potential safety benefit is unknown, at least for a driver assistance system. This because an emergency brake system should only be used when no other options are available, often decided by a threat assessment algorithm. It should not trigger if the driver is still able to steer away from the obstacle or situation. In the case of the velocity gain in 135 km/h, the driver has approximately 100 m of road to use for an avoidance maneuver. It might be too much on the safe side to induce the emergency brake with such a large margin left, where the driver has the possibility to steer away from the obstacle. It has been shown that a driver that stays within his comfort levels can steer away from an accident with a time to collision of  $\sim 1$  s [33]. Comparing that time to the stopping time mentioned for the high speed case tested 135 km/h which was around 3 s shows that an ADAS system utilizing the available width of the road can probably only mitigate crashes at those speeds, since it would only be activated during the last second.

## 7 Conclusions & Future Work

The thesis has evaluated the optimal way of braking while cornering. The results show that by allowing a certain off-tracking the braking distance can be reduced. The significance of this reduction can be questioned since the possible gain is small ( $\sim 1$  m) at low speeds (90 km/h). At higher initial speeds (135 km/h) the gain is larger, reducing the braking distance by around 10 %. An impact speed reduction could also be observed, with a reduction of up to 51 km/h for the case of 135 km/h, by allowing the vehicle to off-track 2 m.

By observing the trivial case of path following it can be concluded that the priority of the motion must initially be shifted towards lateral capability to maintain the specified path. As the velocity decreases, more of the road adhesion budget can be allocated to longitudinal braking of the vehicle. A sensitivity analysis of the scenario showed that to brake optimally, the side slip is of importance. When limiting the allowed side slip, the results were longer braking distances. It could be concluded that this is because the magnitude of the lateral tire forces are of importance to counteract the longitudinal braking forces, when observing their respective contribution to the total yaw moment acting on the vehicle.

A comparison between optimal controlled braking (OBC) and optimal control with optimal steering (OCBS), utilizing the initial states from a steady state cornering, showed the possibility of using the steering to generate the lateral forces needed for following the intended vehicle path. Starting from steady state cornering was however giving a transient behavior. The results from the quasi-steady braking, where the transient was neglected, showed large magnitudes of lateral forces early in the maneuver, which confirms that high lateral forces must be established in order to maximize longitudinal deceleration with constraints of path following. The quasi-steady state brake solution was considered by setting some boundary conditions free. The quasi-steady state solution is therefore considering a maneuver where braking has already been initiated, with small jerks, to is mimicking a real brake intervention. However, the transient phase could be minimized with other methods. Future work could be a more realistic generation of the initial conditions. It could be to start from steady state cornering conditions while adding constraints on yaw acceleration or yaw moment to dampen the transient phase in the beginning of the maneuver.

For future work; an improvement can be achieved regarding the performance of the reference system, FPBS. FPBS has a clear weakness, due to the varying vertical load. It can be improved through implementing a variable brake distribution. The vehicle experience varying load transfer during the scenario and could therefore be improved with a variable brake distribution front/rear to brake according to the vertical load on each axle. A variable brake distribution captures the behavior of EBD, and is a more state of the art system. Future work could also include the use of a fixed optimal steering angle during the maneuver for the reference system to mimic a more realistic driver behavior.

The optimal control of a particle model showed almost identical results compared to the optimal brake control of a two track model with quasi-steady state braking. With this comparison, it can be concluded that a particle model could be useful for path estimation in the case of a braking in corner situation. A simple integrated brake controller (AMR) showed potential when comparing it to the optimal control solution (OCB) and the reference system FBPS. This controller uses a simple acceleration allocation either for longitudinal or lateral priority based on the friction circle and a simple expression for wanted radius derived from the particle representation. However, a future analysis of wanted path radius, based on the optimal lane utilization, must be considered. Future work should therefore include evaluation of the optimal path continuously during the maneuver. This can be done by deriving the optimal path for a particle model from the current location to a standstill continuously, to correct possible deviations from the intended path, thus improve the performance of the AMR controller. Future work could also include using the actual longitudinal allocation factor instead of an expected radius, from the optimal control solution for a particle representation. The AMR controller provides a braking factor that can easily be converted into a force vector angle for implementation with advanced control allocation. The results also indicates that future work of an integrated vehicle motion control including steering could be done to provide the sufficient lateral velocity to control the vehicle via quasi-steady brake solution.

Future work can also include further analysis of the results for optimal controlled individual wheel forces, to receive a better understanding of the problem. A better understanding of the optimal controlled braking forces will also yield a better understanding of the potential use of a particle model for bringing a safety benefit to future vehicles. The future use of an integrated brake controller, that make use of the allowed off-tracking, is showing some potential regarding the gain in braking distance, stopping time and velocity. The control

allocation discussed briefly in the thesis is only actuating the four brake forces on a vehicle. Future work can be done on how to include all available actuators into this kind of control allocation. Including actuators such as steering, torque vectoring and regenerative braking.

## References

- [1] N. National Highway Traffic Safety Administration. Critical Reasons for Crashes Investigated in the National Motor Vehicle Crash Causation Survey (2015).
- [2] A. T. vanZanten. Evolution of Electronic Control Systems for Improving the Vehicle Dynamic Behavior (2002).
- [3] *Vision Zero Initiative*. 2016. URL: <http://www.visionzeroinitiative.com>.
- [4] *European and Road and Safety and Observatory - Annual Accident Report*. 2015. URL: [http://ec.europa.eu/transport/road\\_safety/pdf/statistics/dacota/asr2015.pdf](http://ec.europa.eu/transport/road_safety/pdf/statistics/dacota/asr2015.pdf).
- [5] M. Belin et al. The Vision Zero and its Consequences. *Safety and the Environment in the 21st century, Tel Aviv* (1997, 23-27 November). URL: [http://www.trafikverket.se/contentassets/5e3d8c0eb4e94efd9738cca74b912bf5/vz\\_and\\_its\\_consequenses.pdf](http://www.trafikverket.se/contentassets/5e3d8c0eb4e94efd9738cca74b912bf5/vz_and_its_consequenses.pdf).
- [6] W. Chen et al. *Integrated control of vehicle system dynamics: theory and experiment*. INTECH Open Access Publisher, 2011.
- [7] J. D. Lee et al. Collision warning timing, driver distraction, and driver response to imminent rear-end collisions in a high-fidelity driving simulator. *Human Factors: The Journal of the Human Factors and Ergonomics Society* **44.2** (2002), 314–334.
- [8] A. Kullgren et al. Neck injuries in frontal impacts: influence of crash pulse characteristics on injury risk. *Accident Analysis and Prevention* **32** (2000), 197–205.
- [9] A. Eskandarian. *Handbook of Intelligent Vehicles*. Springer-Verlag London Ltd, 2012, p. 660. ISBN: 0857290843.
- [10] B. Jacobsson et al. *Vehicle Dynamics - Compendium for Course MMF062*. Chalmers University of Technology, 2014.
- [11] R. Rajamani. *Vehicle Dynamics and Control*. Springer US, 2012. ISBN: 9781461414339.
- [12] L. Evans and P. H. Gerrish. Antilock brakes and risk of front and rear impact in two-vehicle crashes. *General Motors R&D Center, Automotive Safety Department, Warren, MI 48090-9055, U.S.A.* **28** (1991), 315–323.
- [13] F. Kost et al. *Driving Stability Systems*. Robert Bosch GmbH, 2005. ISBN: 3-86522-085-1.
- [14] M. Boerboom. Electric Vehicle Blended Braking maximizing energy recovery while maintaining vehicle stability and maneuverability, Master’s Thesis in Chalmers’ Automotive Engineering and in European Master of Automotive Engineering (2015).
- [15] H. B. Pacejka. Tyre and vehicle dynamics. *Butterworth-Heinemann* (2012).
- [16] B. Schick and D. Bunz. Vehicle yaw stability when braking at high cornering speeds. *ATZ worldwide* **106.11** (2004), 8–11.
- [17] M. Klomp, M. Lidberg, and T. J. Gordon. On optimal recovery from terminal understeer. *Proceedings of the Institution of Mechanical Engineers, Part D: Journal of Automobile Engineering* (2014), 0954407013511796.
- [18] H. J. Pesch and M. Plail. The Cold War and the Maximum Principle of Optimal Control. *Optimization Stories. Documenta Mathematica* (2012).
- [19] S. G. Nash and A. Sofer. Linear and nonlinear programming (1996).
- [20] P. E. Rutquist and M. M. Edvall. Propt-matlab optimal control software. *Tomlab Optimization Inc* **260** (2010).
- [21] A. Messac, A. Ismail-Yahaya, and C. A. Mattson. The normalized normal constraint method for generating the Pareto frontier. *Structural and multidisciplinary optimization* **25.2** (2003), 86–98.
- [22] A. Group. *AEB TEST PROCEDURES*. 2012. URL: [http://www.mobileye.com/wp-content/uploads/2013/09/AEB\\_test\\_procedures\\_aug12.pdf](http://www.mobileye.com/wp-content/uploads/2013/09/AEB_test_procedures_aug12.pdf).
- [23] T. A. Johansen and T. I. Fossen. Control allocation—a survey. *Automatica* **49.5** (2013), 1087–1103.
- [24] P. Tondel and T. A. Johansen. “Control allocation for yaw stabilization in automotive vehicles using multiparametric nonlinear programming”. *Proceedings of the American Control Conference*. Vol. 1. Citeseer. 2005, p. 453.
- [25] K. Tagesson et al. “Real-time performance of control allocation for actuator coordination in heavy vehicles”. *Intelligent Vehicles Symposium, 2009 IEEE*. IEEE. 2009, pp. 685–690.
- [26] Y. Gao, M. Lidberg, and T. Gordon. Modified Hamiltonian Algorithm for Optimal Lane Change with Application to Collision Avoidance. *MM Science Journal* MAR 2015 (2015), 576–584.
- [27] A. Albinsson. Online State Estimation in Electrified Vehicles Linked to Vehicle Dynamics (2015).

- [28] A. Kullgren et al. Neck injuries in frontal impacts: influence of crash pulse characteristics on injury risk. *Accident Analysis & Prevention* **32.2** (2000), 197–205.
- [29] Vårdguiden. *Pisksnärtsskada – Whiplashskada*. 2012. URL: <http://www.1177.se/Vastra-Gotaland/Fakta-och-rad/Sjukdomar/Pisksnartsskada---whiplashskada/?ar=True>.
- [30] E. Tomasch et al. “Neck Injury Protection: Potential Cost Savings and Improved Seat Evaluation”. *Transport Research Arena (TRA) 5th Conference: Transport Solutions from Research to Deployment*. 2014.
- [31] W. Castro et al. Do” whiplash injuries” occur in low-speed rear impacts? *European spine journal: official publication of the European Spine Society, the European Spinal Deformity Society, and the European Section of the Cervical Spine Research Society* **6.6** (1996), 366–375.
- [32] M. Krafft et al. How crash severity in rear impacts influences short-and long-term consequences to the neck. *Accident Analysis & Prevention* **32.2** (2000), 187–195.
- [33] M. Brännström, E. Coelingh, and J. Sjöberg. Model-based threat assessment for avoiding arbitrary vehicle collisions. *Intelligent Transportation Systems, IEEE Transactions on* **11.3** (2010), 658–669.

# Appendix

## A Vehicle Data

The vehicle data used in completed simulations, and evaluation of strategies are displayed in Table (A.1). The vehicle data represents a medium-size passenger vehicle of today. The table also displays the parameters used in the simplified tire model used in the thesis.

Table A.1: *Vehicle data and tire characteristics*

Description	Symbol	Value
Vehicle mass [kg]	$m$	1675
Yaw radius of gyration [m]	$k$	1.32
Wheelbase [m]	$L$	2.675
Distance from axle to CoG (front; rear) [m]	$a_1; a_2$	0.4; 0.6
Track width [m]	$w$	1.5
Half track width [m]	$s$	0.75
Height of CoG [m]	$h$	0.5
Lumped lateral load transfer coefficient (front, rear) [-]	$\zeta_1; \zeta_2$	0.17; 0,16
Road friction coefficient [-]	$\mu$	1
Tire data [-]	$C; B$	$\frac{3}{2}; \frac{10}{\mu}$

# B Vehicle System Modelling

## B.1 Coordinate System Transformation

A coordinate transformation of the position of planar vehicle model from the body fixed coordinate system for the vehicle model to the global reference system is performed by utilizing the transformation matrix shows in Expression (B.1).

$$\begin{bmatrix} X \\ Y \end{bmatrix} = \begin{bmatrix} \cos(\psi) & -\sin(\psi) \\ \sin(\psi) & \cos(\psi) \end{bmatrix} \begin{bmatrix} x \\ y \end{bmatrix} \quad (\text{B.1})$$

## B.2 Vehicle Dynamics Theory

The following section describes the modelling of a vehicle including equations of motion, the vertical load distribution due to longitudinal and lateral accelerations. The section is also describing an analytical description of the non-linear tire behavior and the vehicle behavior due to non-linearity and change in vertical load.

### B.2.1 Two Track Model

The two track model is visualized in Figure (B.1). The vehicle model is a planar vehicle model where the equations of motions is derived through standard Newton-Euler theory [17], derived in the body fixed reference frame explained in (2.1) *Coordinate System*.

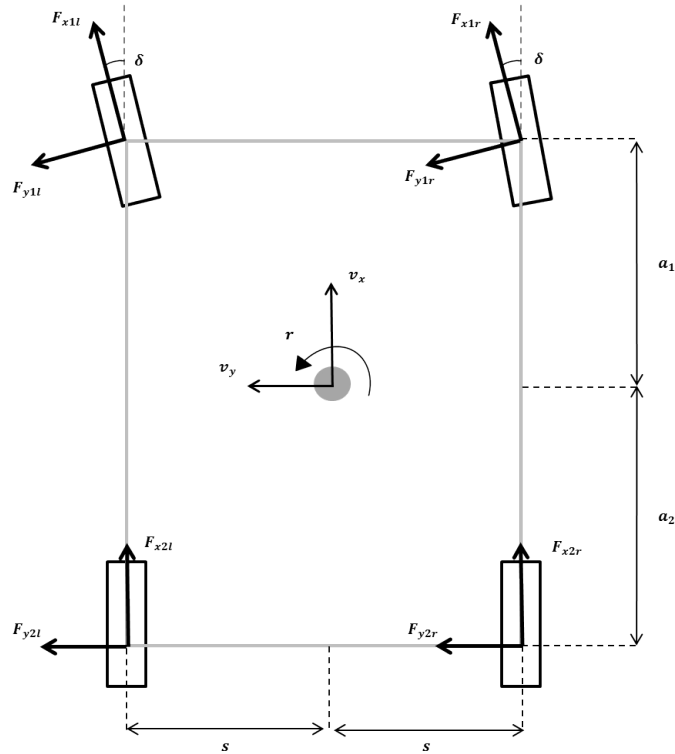


Figure B.1: Freebody diagram for a two track model

The equations of motions, derived from the two track model can be seen in Expression (2.1) to (B.4). The steer angle of the left and right front wheel is assumed to be equal, i.e.  $\delta_{fl} = \delta_{fr} = \delta$

$$\sum F_x : (F_{x1l} + F_{x1r})\cos(\delta) - (F_{y1l} + F_{y1r})\sin(\delta) + F_{2lx} + F_{2rx} = m(\dot{v}_x + rv) \quad (\text{B.2})$$

$$\sum F_y : (F_{y1l} + F_{y1r})\cos(\delta) + (F_{x1l} + F_{x1r})\sin(\delta) + F_{y2l} + F_{y2r} = m(\dot{v}_y - ru) \quad (\text{B.3})$$

$$\begin{aligned} \sum M_z : & ((F_{y1l} + F_{y1r})\cos(\delta) + (F_{x1l} + F_{x1r})\sin(\delta)) \cdot a_1 - (F_{y2l} + F_{y2r}) \cdot a_2 + \\ & + (F_{x2r} + F_{x1r}\cos(\delta) + F_{y1l}\sin(\delta)) \cdot s - (F_{x2l} + F_{y1r}\sin(\delta) + F_{x1l}\cos(\delta)) \cdot s = J\dot{r} \end{aligned} \quad (\text{B.4})$$

## B.2.2 Vertical Load

The vehicle experience load transfer during longitudinal and lateral acceleration. The load transfer is highly affecting the vehicle dynamics due to the non-linearity of the tires. The load transfer is depending on both geometrical (rigid body) and elastic (suspension). The total vertical force is obtained by superposition of the static load and the load transfer due to acceleration and cornering.

### Static Load Distribution

The static load distribution for each wheel is obtained by assuming a fully symmetric vehicle and is shown in Expression (B.5).

$$F_{zij} = \frac{m(L - a_i)}{2L}g \quad i = 1, 2 \text{ and } j = l, r \quad (\text{B.5})$$

### Pitch & Roll Center

The pitch and roll center is defined as the point where the vehicle is pivoting around when experience a longitudinal and lateral acceleration respectively. The roll axis of the vehicle is defined as the axis that connects the front and rear roll centers, that typically is located on different heights. The roll axis is visualized in Figure (B.2). Pivot point for pitch motion can be simplified as the intersection of a vertical axis through the center of gravity and the roll axis.

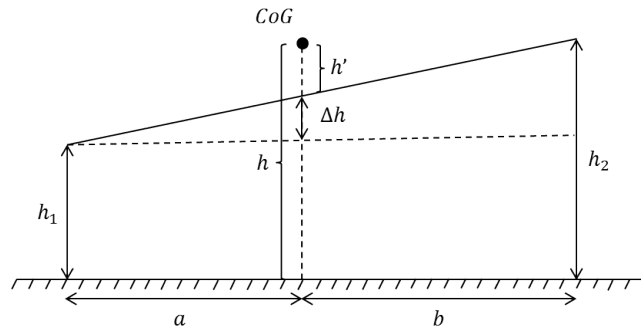


Figure B.2: The roll center axis that connects the front and rear roll center,  $h_1$  and  $h_2$  respectively.  $h'$  is representing the distance from the center of gravity to the roll axis, seen as the radius of gyration.

## Longitudinal Load transfer

When the vehicle is accelerating or decelerating, the vehicle will experience a pitch motion. The pitch will induce forces due to pitch stiffness and damping based the suspension characteristics on the front and rear axle. An dynamic equilibrium for the pitch motion of the body in the pitch center, with The inertial force is assumed to be acting in the center of gravity, yields Expression (B.6).

$$\sum M_y = -(I_{yy} + m_s h'^2) \ddot{\theta} - M_\theta - m a_x h' = 0 \quad (\text{B.6})$$

Where  $M_\theta$  seen in Expression (B.7) describe the forces induced in the suspension can be seen as a resistant moment, assuming small angles and that the vehicle pivot point is the pitch center described in B.2 *Pitch & Roll Center*.

$$\begin{aligned} M_\theta &= 2(C_{z1} \cdot a_1 \theta \cdot a_1 + C_{z2} \cdot a_2 \theta \cdot a_2) + 2(K_{z1} \cdot a_1 \dot{\theta} \cdot a_1 + K_{z2} \cdot a_2 \dot{\theta} \cdot a_2) \\ &= 2(C_{z1} a_1^2 + C_{z2} a_2^2) \theta + 2(K_{z1} a_1^2 + K_{z2} a_2^2) \dot{\theta} \\ &= c_\theta \theta + k_\theta \dot{\theta} \end{aligned} \quad (\text{B.7})$$

Where  $C_{zi}$  = spring coefficient for one wheel at an axle,  $K_{zi}$  = damping coefficient at one wheel,  $c_\theta$  = total pitch stiffness  $k_\theta$  = total pitch damping  $i = 1, 2$ .

The change in vertical load due to longitudinal load transfer is derived from dynamic equilibrium observing the chassis only, by an equilibrium around a contact point between a front wheel and the ground, assuming lateral symmetry of the vehicle. The only horizontal force that is contributing to the moment equilibrium is therefore the inertia force  $m a_x$ , from the body, acting in the pitch center. The pitch center is seen as the point connecting the body and the chassis. The equilibrium Expression can be seen in (B.8).

$$\begin{aligned} \sum M_y &= 2\Delta F_{zi} L + M_\theta - m a_x (h - h') = 0 \\ &= 2\Delta F_z L + c_\theta \theta + k_\theta \dot{\theta} - m a_x (h - h') = 0 \\ \implies \Delta F_{zi} &= \frac{1}{2L} \left( c_\theta \theta + k_\theta \dot{\theta} - m a_x (h - h') \right) \end{aligned} \quad (\text{B.8})$$

At constant longitudinal acceleration or deceleration of the vehicle give that the pitch velocity and acceleration is zero, i.e.  $\ddot{\theta} = \dot{\theta} = 0$  which together with using Expression (B.7) and (B.8) for deriving an expression for the pitch angle yields Expression (B.9).

$$\Delta F_z = \frac{m h}{2L} a_x \quad (\text{B.9})$$

## Lateral Load Transfer

Similar to the pitch motion, the vehicle experience a lateral load transfer when cornering. A dynamic equilibrium around the roll center is obtained in Expression (B.10), assuming small angles.

$$\sum M_\varphi = -(I_{xx} + m h'^2) \ddot{\varphi} - M_\varphi + m h' (a_y) \quad (\text{B.10})$$

Where  $M_\varphi$  describes the resistant moment from the suspension defined by the roll stiffness and the roll damping. An Expression for  $M_\varphi$  is seen in (B.11), assuming a symmetric vehicle and linear spring and damper

characteristics together with small angles.

$$\begin{aligned}
\sum M_\varphi &= 2(C_{zi}s_i\varphi + K_{zi}s_i\dot{\varphi})s_i + C_{\varphi_i}^{aux}\varphi \\
&= (2C_{zi}s_i^2 + c_{\varphi_i}^{aux})\varphi + 2k_{zi}s_i^2\dot{\varphi} \\
&= c_{\varphi_i}\varphi + k_{\varphi_i}\dot{\varphi} \\
\implies c_{\varphi_i} &= 2C_{zi}s_i^2 + C_{\varphi_i}^{aux}, \quad k_{\varphi_i} = 2K_{zi}s_i^2
\end{aligned} \tag{B.11}$$

The change in vertical load due to the roll can be derived by a dynamic equilibrium around the roll center, observing a mass less axle. Assuming that the vehicle is symmetric i.e. center of gravity is in the middle of the track width.

$$\sum M_{xi} = F_{zil}s_i - F_{zir}s_i + M_{\varphi_i} + h_i F_{yi} = 0 \tag{B.12}$$

$$\implies \sum M_{xi} = F_{zil}s_i - F_{zir}s_i + c_{\varphi_i}\varphi + k_{\varphi_i}\dot{\varphi} + h_i F_{yi} = 0 \tag{B.13}$$

$c_{\varphi_i}$  = Total roll stiffness on an axle,  $\varphi$  = Roll angle,  $k_{\varphi_i}$  = Total roll damping,  $\dot{\varphi}$  = roll velocity,  $h_i$  = roll center height on an axle,  $F_{yi}$  = lateral force on an axle. The vertical force can be divided into a static and variable part,  $F_{z_{ij}0}$  and  $\Delta F_{zi}$  respectively where  $i = 1, 2$  and  $j = l, r$ .

$$\implies \sum M_{xi}(F_{zil0} - \Delta F_{zi})s_i - (F_{zir0} + \Delta F_{zi})s_i + c_{\varphi_i}\varphi + k_{\varphi_i}\dot{\varphi} + h_i F_{yi} = 0 \tag{B.14}$$

This lead to that the Expression (B.15) for the variable vertical force, assuming that the vehicle is symmetric. The lateral force is expressed in terms of the lateral acceleration.

$$\Delta F_{zi} = \frac{1}{2s_i} \left( C_{\varphi_i}\varphi + k_{\varphi_i}\dot{\varphi} + \frac{L - a_i}{L} m a_y h_i \right) \quad i = 1, 2 \text{ and } j = l, r \tag{B.15}$$

When the vehicle experience a steady state cornering situation, the roll velocity and acceleration is equal to zero, i.e.  $\ddot{\varphi} = \dot{\varphi} = 0$ . The lateral load transfer is obtained by deriving an expression for the roll angle from Expression (B.10) and (B.11) for steady state cornering. The Expression for the load transfer is seen in (B.15).

$$\Delta F_{zi} = \frac{1}{2s_i} \left( \frac{c_{\varphi_i} h_i}{c_{\varphi_1} + c_{\varphi_2} - m h_i g} + \frac{(L - a_i) h_i}{L} \right) m a_y \tag{B.16}$$

### B.2.3 Tire Dynamics Theory

The only external forces, apart from the aerodynamic forces, that effects a vehicle is the tire forces. These are the main forces that are used to control the vehicle. These forces arises when the tires are experiencing slip.

#### Tire Slip

The longitudinal forces propelling the vehicle is created when torque is applied to the wheels and a speed difference between the wheel speed and the ground speed arises. This is called longitudinal slip,  $\kappa$ , or slip ratio. This slip is defined as a fraction of longitudinal wheel speed in the contact point compared to the wheel center longitudinal speed as can be seen in equation (B.17). This slip is defined differently depending on if the wheel is driven or braked.

$$\kappa_{driven} = \frac{\omega R - v_{x,w}}{|\omega R|}, \quad \kappa_{braked} = \frac{\omega R - v_{x,w}}{v_{x,w}} \tag{B.17}$$

With  $R$  representing the wheel radius,  $\omega$  represents the rotational speed of the wheel and  $v_{x,w}$  is the longitudinal velocity of the wheel in its own local coordinate system.

The slip angle,  $\alpha$ , is what determines the lateral forces of the wheels. It is derived from the lateral slip of the wheel and the steer angle of the wheel. The lateral slip is defined as the wheel lateral speed divided by the wheel longitudinal velocity. For any given wheel the equation for the slip angle becomes:

$$\alpha_{ij} = \delta_i - \text{atan}\left(\frac{v_{y,wij}}{v_{x,wij}}\right) \quad i = 1, 2 \text{ and } j = l, r \quad (\text{B.18})$$

Using equation (B.19) one can calculate the wheel velocities from the vehicle states.

$$\mathbf{v}_{ij} = \mathbf{v}_0 + \boldsymbol{\Omega} \times \mathbf{r}_{ij} \quad i = 1, 2 \text{ and } j = L, R \quad (\text{B.19})$$

Where  $\mathbf{v}_0$  = velocity vector of the origin for the vehicle,  $\boldsymbol{\Omega}$  = Rotational speed around the z-axis and  $r$  = Position vector for the the wheel.

The slip angles are thereafter calculated according to the expression found in (B.20).

$$\begin{aligned} \alpha_{1l} &= \delta_f - \text{atan}\left(\frac{v_y + ar}{v_x - wr}\right), & \alpha_{1r} &= \delta_f - \text{atan}\left(\frac{v_y + ar}{v_x + wr}\right), \\ \alpha_{2l} &= -\text{atan}\left(\frac{v_y - br}{v_x - wr}\right), & \alpha_{2r} &= -\text{atan}\left(\frac{v_y - br}{v_x + wr}\right) \end{aligned} \quad (\text{B.20})$$

## Tire Forces

The amount of longitudinal and lateral force on the wheels can be simplified as a function of the amount of the slip components together with the amount of vertical force and the friction coefficient in the contact patch. The dynamics of tires are however more advanced and they show a non-linear relation to the slip angle which can be seen in figure (B.3)[15]. The figure also displays the effect of combined slip i.e. how longitudinal and lateral slip affects the amount of longitudinal and lateral force the tires can produce. The longitudinal and lateral force is utilizing the same budget in terms of road adhesion, which can be seen in the side force versus brake force diagram.

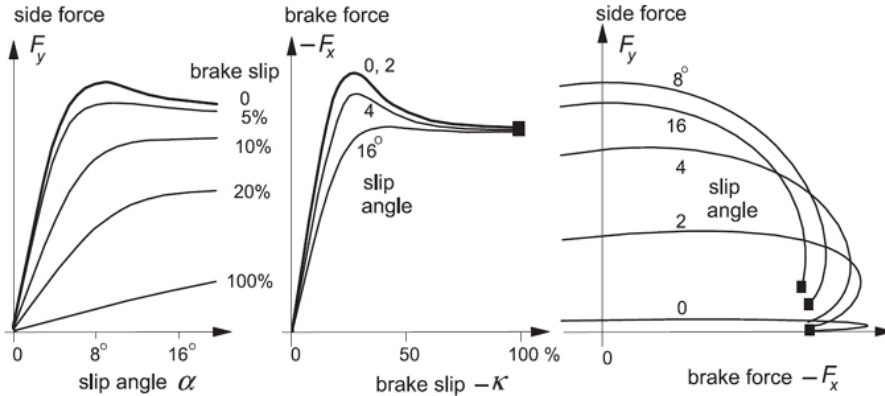


Figure B.3: The tires shows a non-linear degressive behavior. Figure from [15].

From figure (B.3) it can be concluded that the tire cannot produce a larger force after a certain point of slip, i.e. the tire saturates. The behavior of the tires differs between tire to tire, however a common characteristics of saturation can be identified. The modeling of the tire behavior and the non-linearity of the tires is therefore a complex, also considering that different tire behave differently. One well known analytical model of the tire behavior is the *Magic Tire Formula* [15], and is widely used for basic understanding of the tire behavior.

A simplified tire model is shown in expression (B.21). The tire model captures the saturation of the tires but suppresses the decrease in force after exceeding the point saturation. The simplified tire model is well suited for optimization, since a hyperbolic tangent function saturates and converges to a certain value.

$$F_{yij} = D_{yij} \cdot \tanh(C \cdot B \cdot \alpha_{ij}) \quad i = 1, 2 \text{ and } j = l, r \quad (\text{B.21})$$

Where  $D_{ij}$  represents the peak value i.e.  $D_{ij} = \mu F_{zij}$  if pure lateral forces are considered.  $D_{ij}$  can be expressed using simple combined slip model assuming the longitudinal forces as known seen in expression (2.10).

$$D_{yij} = \left( \sqrt{(\mu F_{zij})^2 - F_{xij}^2} \right) \quad i = 1, 2 \text{ and } j = l, r \quad (\text{B.22})$$

Where the longitudinal force is within the range  $\mu F_{zij} \cos(\alpha) \leq F_{xij} \leq \mu F_{zij}$ .

The tire behavior can be modelled as linear when operating in the region of small slip angles. The linear tire region is called cornering stiffness,  $C_{F\alpha}$ . The Cornering stiffness is defined by  $C_{F\alpha} = \left. \frac{dF_i}{d\alpha_i} \right|_{\alpha_i=0} = BCD$ .

## B.2.4 Vehicle Behavior

When the vehicle is braking or is traveling in a corner it experience a load transfer, both due to geometrical relations and due to forces through the suspension, i.e. due to the roll and pitch angles. The load transfer is affecting how the amount of lateral force that can be produced on each axle due to characteristics of the vehicle, regarding roll stiffness, spring stiffness and damping characteristics. Load transfer reduces the effective cornering stiffness on the axles as seen in figure (B.4) [15]. The loss of cornering capability can be seen as the additional slip angle,  $\Delta\alpha$ , that has to be produced to reach the same amount of lateral force.

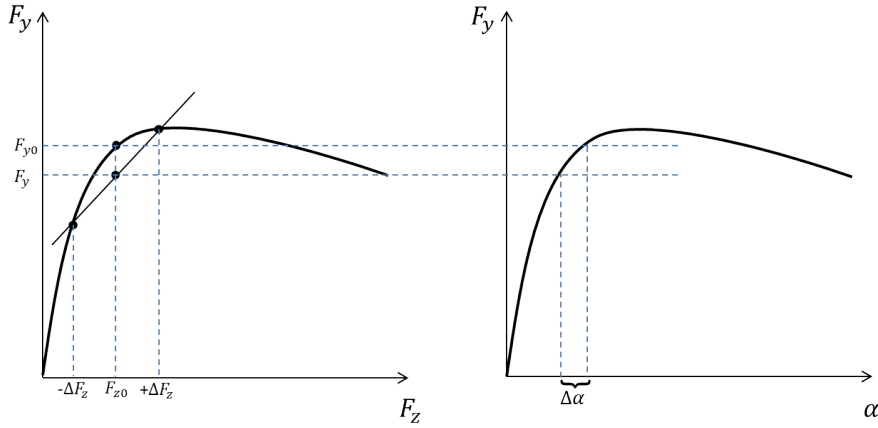


Figure B.4: Reduction of effective cornering stiffness due to load transfer

In cases with an oversteering vehicle it is the rear axle that has reduced its effective cornering stiffness the most i.e. cannot produce enough lateral force to keep the vehicle stable. If the vehicle is understeering it shows that it is the front axle that lost grip and thereby cannot produce enough lateral force to move the vehicle as the desired path. Thus, it is the non-linearity of the tires are affecting the vehicle behavior and thereby the stability and maneuverability of the vehicle.

## B.2.5 Ideal Braking distance, Effective Curve Radius & Actual Curve Radius

Ideal braking distance is described as the shortest braking distance that can be achieved assuming that all utilized road adhesion is used for longitudinal deceleration during the maneuver. The theoretical braking

distance is calculated via the energy law, where and braking force works as a non-conservative force.

$$\Delta W + \Delta T = W^{ik} \quad (\text{B.23})$$

$$T_1 = \frac{mu^2}{2} \quad (\text{B.24})$$

$$T_2 = 0 \quad (\text{B.25})$$

$$\Delta W = 0 \quad (\text{B.26})$$

$$W^{ik} = F_{brake} \cdot x_{long} = \mu mg \cdot x_{long} \quad (\text{B.27})$$

$$\frac{mu^2}{2} = \mu mg \cdot x_{long} \quad \implies x_{long} = \frac{u^2}{2\mu g} \quad (\text{B.28})$$

The effective curvature is derived from assuming the steady state cornering according to Expression (B.29).

$$\kappa = \frac{r}{v_x} \quad (\text{B.29})$$

The measurement of the actual curve radius over a time history can be derived from using the vehicle states  $v_x$  and  $v_y$  and the acceleration magnitude during over the time history. The Expression for the actual curve radius is seen below:

$$\kappa = \frac{v_x \cdot a_y - v_y \cdot a_x}{(v_x^2 + v_y^2)^{3/2}} \quad (\text{B.30})$$

## C Sensitivity Analysis Regarding Side Slip & Friction Variations

A sensitivity study for the quasi-steady results was done in with respect to allowing a variation of side slip. The side slip constraint was set to  $\max(|\beta(t)|) \leq 5^\circ$ ,  $10^\circ$  and  $20^\circ$  and the variation in braking distance for the optimal braking solution can be seen in table (C.1)

Table C.1: *The braking distance can be decreased by allowing a larger slip angle during the scenario for a road adhesion level of  $\mu = 1$ .*

$d_{off}$ m	0.05	0.5	1	2
90 km/h	33.2 <sup>a</sup> m	32.7 <sup>a</sup> m	32.4 <sup>a</sup> m	31.8 <sup>a</sup> m
	32.8 <sup>b</sup> m	32.4 <sup>b</sup> m	32.1 <sup>b</sup> m	31.7 <sup>b</sup> m
	32.8 <sup>c</sup> m	32.4 <sup>c</sup> m	32.1 <sup>c</sup> m	31.7 <sup>c</sup> m
120 km/h	67.2 <sup>a</sup> m	65.0 <sup>a</sup> m	63.5 <sup>a</sup> m	61.4 <sup>a</sup> m
	64.1 <sup>b</sup> m	62.6 <sup>b</sup> m	61.5 <sup>b</sup> m	59.9 <sup>b</sup> m
	63.9 <sup>c</sup> m	62.4 <sup>c</sup> m	61.4 <sup>c</sup> m	59.8 <sup>c</sup> m
135 km/h	101.3 <sup>a</sup> m	92.2 <sup>a</sup> m	88.3 <sup>a</sup> m	83.7 <sup>a</sup> m
	94.1 <sup>b</sup> m	89.01 <sup>b</sup> m	86.1 <sup>b</sup> m	82.3 <sup>b</sup> m
	93.8 <sup>c</sup> m	88.8 <sup>c</sup> m	85.9 <sup>c</sup> m	82.2 <sup>c</sup> m

<sup>a</sup> Optimal braking with side slip constraint,  $\max(|\beta(t)|) \leq 5^\circ$

<sup>b</sup> Optimal braking with side slip constraint,  $\max(|\beta(t)|) \leq 10^\circ$

<sup>c</sup> Optimal braking with side slip constraint,  $\max(|\beta(t)|) \leq 20^\circ$

A decrease in braking distance can be observed due to the increase of the maximum side slip value. The difference in braking distance between the different allowed off-tracking magnitudes are more pronounced at higher initial velocities. The biggest difference is observed from the case of 135 km/h at the most strict path following case of 0.05 m where the actual decrease in braking distance amounts to 7.5 m comparing  $\max(|\beta(t)|) \leq 5^\circ$  and  $\max(|\beta(t)|) \leq 20^\circ$ . The reduction of braking distance becomes less obvious for the step from  $\max(|\beta(t)|) \leq 10^\circ$  to  $\max(|\beta(t)|) \leq 20^\circ$ . This relation can be explained by that small levels of side slip reduces the possible slip angles of the tires. This reduces the lateral tire force capabilities and the turn in moment. This reduction means that the longitudinal braking forces which creates a turn out moment needs to be reduced to balance the total yaw moment. A more knowledge rewarding analysis was done observing the force vector angle in the different cases of imposed side slip constraints, which showed as similar results of how the braking maneuver should be performed. The force vector angles for the case of 90 and 135 km/h in a corner with an allowed off-tracking of 0.5 m is displayed in figure (C.1).

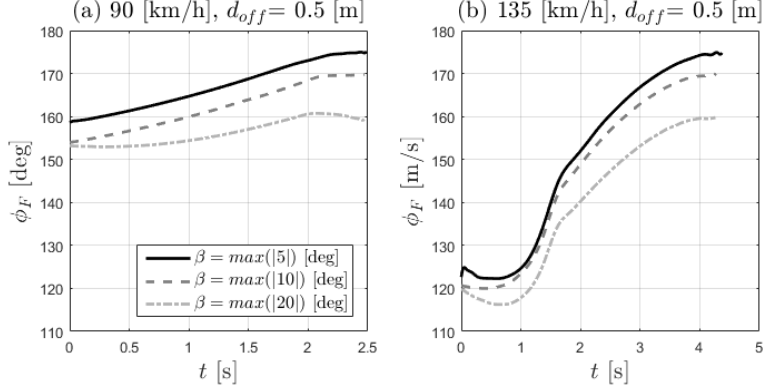


Figure C.1: (a) force vector angle of the case of 90 km/h and (b) force vector angle of the case of 135 km/h for a corner radius of 150 with an allowed off-tracking of 0.5 m with varying side slip constraints.

The force vector angle shows a minor variation in how the brake intervention is performed, with respect to the used initial boundary conditions, when allowing a certain slip angle. The peak value of the force vector angle and the allowed slip angle correlates well, seen as that the force angle reaches different peak values. The case of imposed side slip constraint of  $\max(|\beta(t)|) \leq 5^\circ$  reaches a final angle of  $175^\circ$  while the case of imposed  $\max(|\beta(t)|) \leq 20^\circ$  approaches  $160^\circ$ . All peak values is therefore correlating to that the force vector is applied in the opposite direction of the velocity vector, i.e. full utilization of road adhesion to stop the vehicle in the end of the maneuver for both initial velocity cases and all imposed side slip constraints. A similar comparison as for the side slip variation was performed for the case of changing the road conditions defined by the friction coefficient. The friction coefficient was changed to  $\mu = 0.5$  during the entire path and the results for an imposed side slip constraint of  $\max(|\beta(t)|) \leq 5^\circ$  and  $\max(|\beta(t)|) \leq 10^\circ$  was used during the evaluation. A comparison of braking distance between  $\max(|\beta(t)|) \leq 5^\circ$  and  $\max(|\beta(t)|) \leq 10^\circ$  when experiencing a lower road adhesion is done in Table (C.2)

Table C.2: The braking distance can be decreased by allowing a larger slip angle during the scenario for a road adhesion level of  $\mu = 0.5$ .

$d_{off}$ m	0.05	0.5	1	2
90 km/h	75.8 <sup>a</sup> m	73.5 <sup>a</sup> m	71.8 <sup>a</sup> m	69.5 <sup>a</sup> m
	75.5 <sup>b</sup> m	73.2 <sup>b</sup> m	71.6.1 <sup>b</sup> m	69.4 <sup>b</sup> m

<sup>a</sup> Optimal braking with side slip constraint,  $\max(|\beta(t)|) \leq 5^\circ$

<sup>b</sup> Optimal braking with side slip constraint,  $\max(|\beta(t)|) \leq 10^\circ$

The braking distance comparison for a road adhesion level of  $\mu = 0.5$ , between the an imposed side slip constraint of  $\max(|\beta(t)|) \leq 5^\circ$  and  $\max(|\beta(t)|) \leq 10^\circ$  shows similar trends as for the cases with a road adhesion level of  $\mu = 1$ . It can be concluded that the braking distance is sensitive to magnitude of the side slip. However, the differences in braking distance for different side slip constraints tend to decrease with a lower road adhesion level. The velocity limit decreases with road adhesion level, as discusses above, and for the case of  $\mu = 0.5$  the velocity limit becomes  $v_{lim} = 98$  km/h. It is therefore concluded that the initial velocity is closer to the velocity limit and the behavior of the braking forces differs between the comparison between the initial velocity of 90 km/h for a road adhesion of  $\mu = 0.5$  and  $\mu = 1$ . The difference of the time history of force vector angle between the variation in road adhesion and side slip constraints can be seen in Figure (C.2).

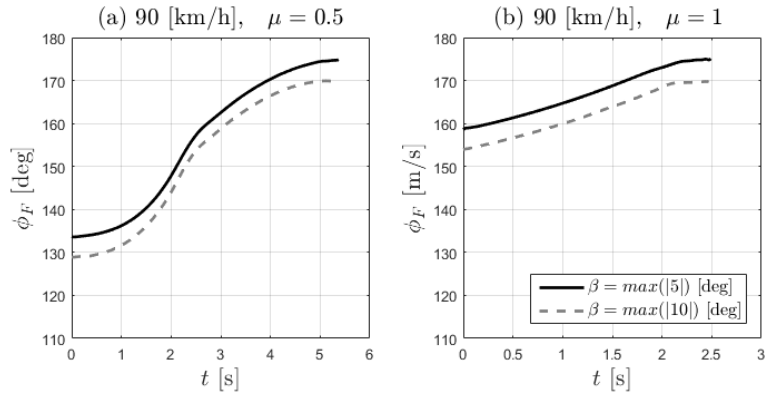


Figure C.2: Force vector angle of the case of 90 km/h in a corner radius of 150 with an allowed off-tracking of 0.5 m

From Figure (C.2) it can be concluded that a natural difference appears between the different road adhesion levels. However, the overall strategy of prioritizing lateral capability initially remains. By comparing the force vector angle results for the variation of road adhesion and side slip constraints it can be concluded that the same trends can be seen regarding the overall procedure.